R-99-07

A RESISTANCE MODEL FOR EVALUATING INTERACTIONS BETWEEN NATURAL ORGANIC MATTER (NOM) AND MEMBRANES AT DIFFERENT SCALES OF OPERATION

DESALINATION RESEARCH & DEVELOPMENT PROGRAM REPORT NO. 44

September 1999

U.S. DEPARTMENT OF THE INTERIOR
Bureau of Reclamation

Technical Service Center
Civil Engineering Services
Water Treatment Engineering & Research
Denver, Colorado

University of Colorado
Boulder, Colorado

REPORT DOCUMENTATION PAGE

Form Approved
OMB No 0704-0188

1. AGENCY USE ONLY *(Leave Blank)*	2. REPORT DATE	3. REPORT TYPE AND DATES COVERED
	September 1999	Final

4. TITLE AND SUBTITLE
4 Resistance Model for Evaluating Interactions Between Natural Organic Matter andi Membranes at Different Scales of Operation

5. FUNDING NUMBERS

6. AUTHOR(S)
Scott Irvine and Gary Amy (University of Colorado)

7. PERFORMING ORGANIZATION NAME(S) AND ADDRESS(ES)
Bureau of Reclamation
Technical Service Center
Denver, CO 8022.5

8. PERFORMING ORGANIZATION REPORT NUMBER
R-99-07

9. SPONSORING/MONITORING AGENCY NAME(S) AND ADDRESS(ES)
Bureau of Reclamation
Denver Federal Center
PO Box 25007
Denver CO 80225-0007

10. SPONSORING/MONITORING AGENCY REPORT NUMBER
DesalR&D No. 44

11. SUPPLEMENTARY NOTES
Microfiche and hard copy available at the Technical Service Center, Denver, Colorado

12a. DISTRIBUTION/AVAILABILITY STATEMENT
Available from the National Technical Information Service, Operations Division, 5285 Port Royal Road, Springfield, Virginia 22161

12b. DISTRIBUTION CODE

13. ABSTRACT *(Maximum 200 words)*

This research evaluated and compared natural organic matter (NOM) fouling of membranes at different scales of operation. The approach was to interpret NOM fouling in terms of NOM-membrane interactions. Two different sources of surface water and two different membranes were tested to provide variation in the intrinsic properties which affect NOM-membrane interactions. Each water-membrane combination was tested at three different scales of operation. Permeate flux declined through time due to the development of a NOM gel layer on the membrane surface.

A mathematical gel-resistance model was developed to analyze the NOM-membrane interactions and compare the test results at different scales of operation. The model includes parameters related to properties of the NOM, membrane, and feedwater. NOM was characterized in terms of molecular weight distribution and aromatic structure. Measured feedwater properties included pH, conductivity, and concentration of dissolved organic carbon. Membranes were characterized in terms of molecular weight cutoff of the pores, surface charge, and hydrophobicity. Application of the gel resistance model to the membrane test results indicates that properties of the NOM, membrane, and feedwater can be quantitatively related to NOM fouling and permeate flux decline.

14. SUBJECT TERMS--
natural organic matter/NOM/membrane fouling/resistance model/NOM-membrane interactions/pilot tests/bench tests/membrane performance/flux decline/NOM fouling

15. NUMBER OF PAGES
133

16. PRICE CODE

17. SECURITY CLASSIFICATION OF REPORT	18. SECURITY CLASSIFICATION OF THIS PAGE	19. SECURITY CLASSIFICATION OF ABSTRACT	20. LIMITATION OF ABSTRACT
UL	UL	UL	UL

R-99-07

A RESISTANCE MODEL FOR EVALUATING INTERACTIONS BETWEEN NATURAL ORGANIC MATTER (NOM) AND MEMBRANES AT DIFFERENT SCALES OF OPERATION

Desalination Research and Development Program Report No. 44

Scott Irvine
Technical Service Center
Bureau of Reclamation
Denver, Colorado

Gary Amy, Ph.D.
University of Colorado at Boulder
Boulder, Colorado

September 1999

ACKNOWLEDEGMENTS

I would like to express my gratitude to my thesis advisor, Gary Amy, and thesis committee members, Scott Summers and John Pellegrino, for their inspiration and guidance. I am also grateful to my employer, the U.S. Bureau of Reclamation (Reclamation), through which this research effort was funded in its entirety. I am thankful to the following individuals for the considerable assistance I received in conducting membrane tests:

- Jaeweon Cho, and Yeomin Yoon, researchers at the University of Colorado at Boulder
- Tom Bunnelle. technician at Reclamation's Denver laboratory
- The staff at Reclamation's Water Quality Improvement Center in Yuma, Arizona

EXECUTIVE SUMMARY

This research evaluated and compared NOM fouling of membranes at different scales of operation. The approach of this research was to interpret NOM fouling in terms of NOM-membrane interactions. Two different sources of surface water and two different membranes were tested to provide variation in the intrinsic properties which affect NOM-membrane interactions. Each water-membrane combination was tested at three different scales of operation. Permeate flux declined through time and was attributed to the development of a NOM gel layer on the membrane surface.

A mathematical gel-resistance model was developed to analyze the NOM-membrane interactions and compare the test results at different scales of operation. The model includes parameters related to properties of the NOM, membrane, and feedwater. NOM was characterized in terms of molecular weight (MW) distribution and aromatic structure. Measured feedwater properties include pH, conductivity, and concentration of dissolved organic carbon (DOC). Membranes were characterized in terms of molecular weight cutoff (MWCO) of the pores, surface charge, and hydrophobicity.

Application of the gel resistance model to the membrane test results indicates that properties of the NOM, membrane, and feedwater can be

quantitatively related to NOM fouling and the resulting permeate flux decline at each scale of testing. These quantitative relationships were observed at different scales of testing: however, each scale of membrane operation imposes unique operating conditions that also influence the test results, The gel resistance model also provided a means for interpreting the differences in test results due to the operational differences between each scale of testing. The utility of the model lies in its potential use as a tool for predicting NOM fouling and membrane performance at larger scales of operation.

CONTENTS

TABLES

FIGURES

1 .O INTRODUCTION

The relevance of NOM to membrane treatment of drinking water is two-fold:

1) During water treatment, chemical disinfectants used to destroy pathogens react with NOM to form hazardous disinfection by-products (DBPs) which are regulated under U.S. EPA primary drinking water regulations. Proposed regulations would require some water treatment utilities to reduce NOM levels because they are precursors to DBP formation. Reverse osmosis, nanofiltration, and to a lesser extent, ultrafiltration membranes are effective in removing NOM, but they are also susceptible to fouling as the NOM accumulates on and within the membrane surface.

2) NOM is ubiquitous in drinking water supplies (especially surface waters) and, therefore, frequently a source of fouling during membrane treatment. NOM accumulates on and reduces the flux through membranes with an effective pore size similar to or smaller than NOM molecules (e.g., about 2000 relative molecular mass). Membranes of this porosity include reverse osmosis, nanofiltration, and some tight ultrafiltration membranes. Typical pretreatment operations such as coagulation, filtration, pH adjustment, and disinfection are used to

remove other types of foulants but they are usually not adequate to control NOM.

Bench- and pilot-scale studies are the principal means for predicting permeate flux decline and overall membrane performance at larger scales of operation. The results of these studies provide the basis for membrane selection, developing operation procedures, and estimating treatment cost. Bench- and pilot-scale studies are now required under the U.S. EPA Information Collection Rule (ICR) (1996a) for all water treatment plants and utilities that serve over 100,000 persons (over 50,000 persons for groundwater treatment plants) having an annual average total organic carbon (TOC) content greater than 4.0 mg/L (greater than 2.0 mg/L for groundwater treatment plants). The purpose of this mandate is to obtain information on the cost and feasibility of advanced water treatment to reduce the level of DBP precursors (i.e., NOM measured as TOC).

The objective of this research was *to* compare and contrast NOM fouling at different scales of membrane operation. A mathematical model was developed to provide a tool for analyzing the NOM-membrane interactions that influence NOM fouling and the resistance to permeate flow. This resistance model also provides another means of predicting membrane perfonance at larger scales of operation, which is also a goal of the ICR effort.

2.0 BACKGROUND AND LITERATURE REVIEW

2.1 Factors that Influence NOM Fouling

Development of a gel resistance model requires an understanding of the factors related to NOM fouling. Considerable research in this area has revealed that the NOM accumulation at the membrane surface is dependent on operating parameters (e.g., pressure, feedwater velocity) and properties of the NOM, feedwater, and membrane (Cho, 1998).

Nanofiltration and ultrafiltration are pressure-driven processes, in which water is forced to permeate the small membrane pores by the application of pressure. The permeate flux rate is generally proportional to the applied pressure until the accumulation of solutes in the concentration-polarization layer reaches a threshold concentration that limits further increases in flux (Porter, 1972).

The amount or thickness of solute accumulation is also dependent on the flow hydrodynamics at the membrane surface. Increasing the Reynolds number of the flow produces greater shear at the membrane surface causing a reduction in the amount of foulant material (Porter, 1972). A research study evaluated nanofiltration using a stirred cell test apparatus and found that decreasing the stirring speed caused a pronounced increase in concentration

polarization and NOM deposition on the membrane surface (Schafer, et al., 1998). Various empirical correlations have been proposed to describe solute concentration in the concentration-polarization layer as a function of the flow velocity and channel geometry (Chapman-Wilbert, et al., 1998).

A lower concentration of NOM in the feedwater suggests that the rate of accumulation of NOM at the membrane surface will be slower and that less fouling will occur in a given time period. A nanofiltration study found a proportional relationship between the mass of NOM foulant and the NOM concentration in the feedwater (DiGiano, 1997). The size of solute foulants relative to the pore size of the membrane is also a determining factor in the amount of solute that is rejected by the membrane. NOM macromolecules that are larger than the membrane pores will accumulate at the membrane surface where they are subject to hydrophobic and electrostatic interactions (Fu, et al., 1994).

Particles and solutes that foul in an aqueous medium tend to be hydrophobic. Increasing hydrophobic character of the NOM and/or membrane results in greater NOM adsorption on the membrane surface. Hydrophobic NOM tends to aggregate as colloids because this lowers the interfacial free energy (surface tension) due to surface area exposure. Hydrophobic NOM favors attachment to any membrane material less hydrophilic than water because less exposure can be achieved by attachment

to this surface. The hydrophobicity of a membrane can be characterized by measuring the angle of contact between the membrane and a drop of water on its surface (Zhang, et al., 1989).

NOM is comprised of a mixture of humic and non-humic fractions, the former comprised of humic and fulvic acids. The hydrophobic character of NOM resides primarily within the humic/fulvic acid fraction (Jucker and Clark, 1994; Nilson and DiGiano, 1996). The humic content of a water can be described by its specific ultraviolet absorbance (SUVA). SUVA is defined as ultraviolet absorption at 254 nm divided by the dissolved organic carbon (DOC) concentration. Typically, SUVA at <3 L/mg•m indicates largely non-humic (nonhydrophobic) material, whereas SUVA in the range of 4 - 5 L/mg•m indicates mainly humic material (Krasner, et al., 1999).

Electrostatic interactions between the NOM, membrane, and dissolved ions in the feedwater are a significant factor in NOM fouling. There is a natural electrostatic repulsion between negatively-charged NOM and a negatively-charge membrane. Previous studies have shown that NOM fouling increases at low pH and high ionic strength of the feedwater as a result of charge neutralization, electric double layer compression, and NOM complexation with dissolved ions (Schafer, et al., 1998; Braghetta, et al., 1998; Braghetta, et al., 1997).

2.2 Comparison of Different Scales of Membrane Operation

Laboratory, bench- and pilot-scale membrane studies are conducted on the basis that test results can be extrapolated to predict performance at larger scales of operation. Federal regulations have been promulgated which require some utilities to conduct bench- and pilot-scale studies for water treatment (U.S. Environmental Protection Agency, 1996a; 1996b). Under these circumstances it is important to compare and evaluate NOM fouling at different scales of membrane operation. A project will be undertaken to gather membrane operation data from full-scale membrane plants and previously conducted pilot-scale studies to study their correlation (Allgeier, 1999).

Several studies have been completed that compare membrane performance at different scales of operation. The New Jersey-American Water Company conducted bench- and pilot-scale ICR studies of nanofiltration treatment of surface water from the Passaic River in Millburn, New Jersey (Ibrahim, et al., 1999). Comparison of the test results showed a 7% difference in the rejection of NOM between the bench and pilot scale. Another study found that differences in membrane flux and rejection characteristics between the bench and pilot scale can be caused by variations in the membrane material inherent in the manufacturing process

(Gusses, 1999). The authors also concluded that bench-scale test results should be representative of short-term performance at the pilot scale.

Nanofiltration of lake water and river water was compared at the bench and pilot scales in two separate studies in Cincinnati, Ohio (Gusses, 1996; Gusses, 1997). The membrane systems were operated at the same average pressure, crossflow velocity, and recovery in each study. The specific fluxes, amount of flux decline, and rejection characteristics were approximately the same at each scale of operation in both of the studies.

Most studies have shown a good correlation between membrane performance at different scales of operation; however, there are exceptions., A study conducted at Palm Coast, Florida compared the performance of a pilot facility to a full-scale treatment plant using nanofiltration of groundwater (Mulford and Taylor, 1997). The researchers concluded that the pilot facility did not accurately predict the production decline of the full scale plant.

2.3 Mathematical Modeling of NOM Fouling

Relatively few studies have explored mathematical modeling of NOM fouling. The AWWA Membrane Technology Research Committee recently reported that “modeling of adsorptive fouling of membranes by NOM has progressed little...” (American Water Works Association [AWWA], 1998).

Perhaps this is due to the large quantity and complexity of the parameters that affect NOM fouling. One notable effort involved development of a computer program to evaluate membrane performance in terms of operating parameters and membrane configuration (Van der Meer, et al., 1997). The program numerically solved a series of simultaneous equations with about 30 different parameters to model and optimize membrane productivity; however, the model did not include parameters to evaluate flux decline due to NOM fouling.

Another study used a similar approach with comparable complexity to evaluate nanofiltration flux decline caused by NOM fouling (Tu, et al., 1997). The resulting computer program calculates flux decline as a function of operating parameters but does not account for the influence of NOM-membrane interactions on NOM fouling.

3.0 OBJECTIVES

The principal objectives of this research are as follows:

- Develop a mathematical model of NOM fouling with respect to the influence of NOM-membrane interactions.

- Evaluate and calibrate the NOM fouling model by applying it to actual membrane filtration tests.

- Utilize the model to evaluate and correlate NOM fouling at three different scales of membrane operation.

4.0 EXPERIMENTAL METHODS AND ANALYSES

Membrane filtration tests were conducted using two source waters and two membranes at three scales of operation. The amount and rate of NOM fouling depends on properties of the source water, NOM, and membrane as well as the operational conditions imposed by the test apparatus. The laboratory analyses of these properties and the experimental methods for membrane testing are described below.

4.1 Source Waters

Two sources of feedwater were employed to provide variation in the NOM-feedwater properties which influence NOM fouling:

- Surface water from Horsetooth Reservoir (HT water) west of Fort Collins, Colorado. Horsetooth Reservoir receives water from the Colorado-Big Thompson Project which diverts water from the Colorado River on the western slope of the Continental Divide.

- Surface water from the Colorado River (CR water) at Yuma, Arizona.

The average values of various water quality parameters for each of the source waters are shown in Table 4.1.

Table 4.1 Average Composition of Source Waters

Parameter	Unit	HT Water*	CR Water**
pH	units	7.3	8.1
Ca	mg/L as $CaCO_3$	22	78
Mg	mg/L	1.4	29
Na	mg/L	1.9	100
K	mg/L		3.8
HCO_3	mg/L as $CaCO_3$	--	140
SO_4	mg/L	2.9	271
Cl	mg/L	1.1	84
SiO_2	mg/L	2.9	9.3
TDS	mg/L	42	670
Turbidity	NTU	2.5	2.2

*Provided by City of Fort Collins water.
**Provided by Yuma Desalting Plant

4.1.1 Pretreatment of Source Waters

Evaluation of NOM fouling requires the removal or treatment of other potential sources of membrane fouling such as suspended particles, colloids, bacteria:, and algae from the feedwater stream. The total organic carbon (TOC) content of a water is comprised of both dissolved and particulate fractions. The dissolved organic carbon (DOC) fraction consists of macromolecules of NOM that vary in size, structure, and charge; however, their maximum size is considered to be about 0.45 μm. NOM fouling that results from particulate carbon (>0.45 μm) is referred to as the 'cake layer'

whereas NOM fouling that results from dissolved carbon (<0.45 μm) is referred to as the "gel layer." For all tests conducted, both feedwaters were pretreated with a microfilter (0.30 - 0.45 μm, depending on availability) to remove particulate carbon and other potential foulants that are larger than dissolved NOM.

Scaling of the membrane surface can occur as dissolved salts become more concentrated in the reject stream. Also, dissolved biological matter in the feedwater may attach to and grow on the membrane or feed spacer which leads to biofouling. These contaminants are not a concern for laboratory or bench-scale tests which operate at low recovery for a relatively short period of time. Both scaling and biofouling are possible problems during pilot tests which operate for longer time periods at a higher recovery.

Among the two feedwaters, only CR water has a positive Langelier saturation index which indicates a potential for scaling. Therefore, the CR water was pretreated with sulfuric acid to reduce the pH to 7.0 for pilot tests to avoid scaling. Both HT and CR feedwaters were disinfected using chloramines at a dosage of about 1 mg/L to minimize biofouling of the membranes. The above pretreatment of feedwaters was deemed adequate to ensure that observations of flux decline could be primarily attributed to NOM fouling.

4.1.2 Characterization of Feedwaters and NOM

The feedwaters were characterized with respect to electrostatic properties. A temperature-compensated pH probe was used to measure the concentrations of hydronium and hydroxyl ions that result from the dissociation of water molecules. The ionic strength or total dissolved solids (TDS) of the feedwaters was approximated using a conductivity meter to measure their ability to conduct a current.

The amount and character of NOM varies between feedwaters. The amount of NOM was measured as the concentration of DOC. A carbon analyzer (TOC-5000, Shimadzu) was used to measure the DOC content of the water samples. The hydrophobic fraction of DOC was measured as the fraction of total NOM that adsorbed onto XAD-8 resin (Rohm and Haas, Philadelphia) using an acidified sample of feedwater. Ultraviolet absorbance (UVA) of NOM at 254 nm was measured using a spectrophotometer (UV-160A, Shimadzu). The ratio UVA_{254}/DOC is defined as the specific absorbance (SUVA) and provides an index of the humic content and, therefore, the hydrophobic character of the NOM. The molecular weight (MW) distribution of the NOM macromolecules was measured using a high-pressure, size-exclusion chromatograph (SPD-GA, Shimadzu) with a Waters Protein-Pak 125 column calibrated with polystyrene sulfonates.

4.2 Membranes

Two different membranes were used to provide variation in the membrane properties that affect NOM fouling:

- Hydranautics 2540-UST-ESNA nanofiltration membrane (ESNA).
- Desal GM-2540F1078 ultrafiltration membrane (GM).

4.2.1 Characterization of Membranes

Membrane properties that influence NOM-membrane interactions include surface charge, hydrophobicity, and pore size. A commercial electrokinetic measurement apparatus (EKA, Brookhaven Instruments Corp.) was used to measure the zeta potential of the membrane surface. The zeta potential provides an index of the membrane's surface charge. The contact angle between a drop of water and the membrane surface provides an indication of the hydrophobic character of the membrane. The contact angles were measured with a goniometer using the sessile drop method (Zhang et al., 1989).

Differences in pore size between the two membranes were approximated by their molecular weight cutoff (MWCO). The MWCO of the membrane was determined by the membrane manufacturer by filtering a wide size-range of non-charged polyethylene glycols (PEG) through the

membrane. The MWCO of each membrane is defined as the MW of the PEG that is 90% rejected by the membrane.

4.3 Membrane Testing Apparatus

The membranes and source waters described above were tested at three different scales of operation:

- Laboratory stirred cell
- Bench scale
- Pilot scale

4.3.1 Laboratory Stirred Cell Tests

The feedwater was filtered through a membrane disk specimen within a pressurized 200-mL cylinder. A stirring propeller within the cylinder was used to impart an angular flow across the membrane disk to simulate the hydrodynamics in the bench- and pilot-scale tests. A schematic of the stirred cell test apparatus is shown in Figure 4-l.

The stirred cell was operated in similar fashion to the standard procedure for determination of the modified fouling index (Taylor and Jacobs, 1996). A continuous stream of pretreated feedwater from a 2-liter reservoir was applied under pressure to the membrane disk in a dead-end filtration mode causing the retentate to remain within the cylinder during this dead-end

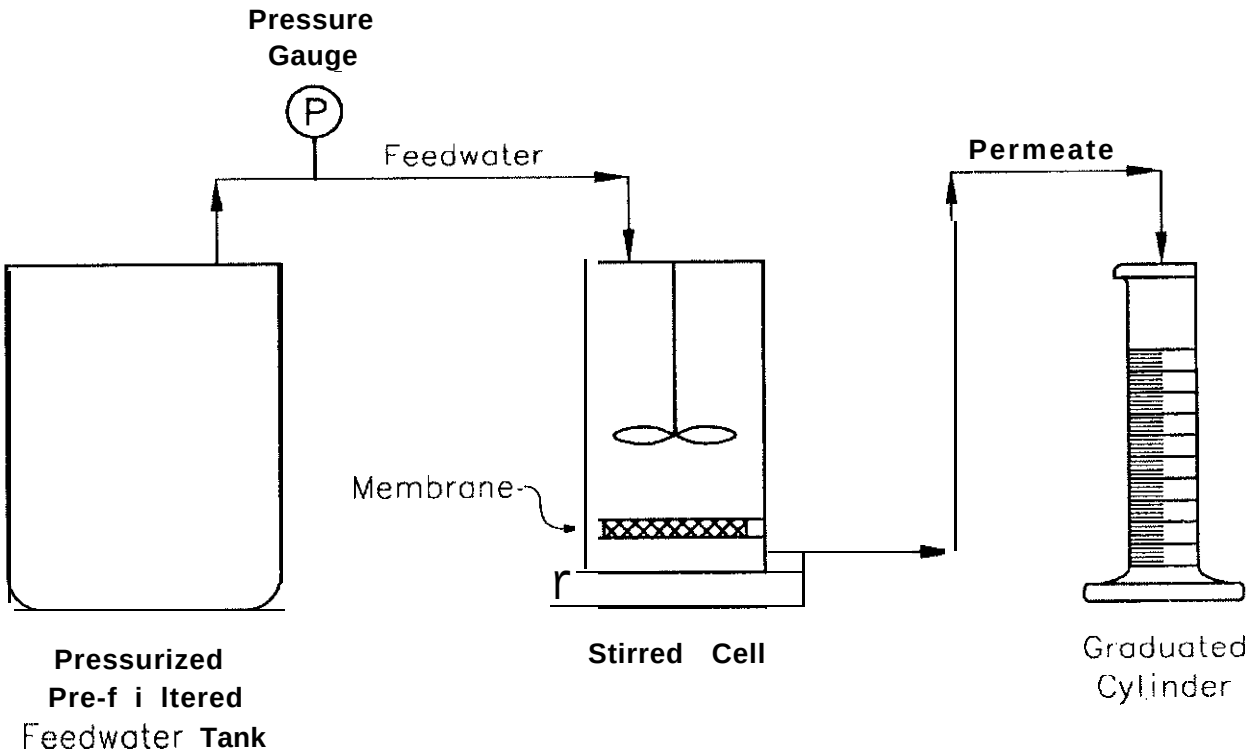

Figure 4.1 - Flow Schematic for Stirred Cell Tests

filtration test. The retained solute mixed with the incoming feedwater which caused the NOM concentration within the stirred cell to steadily increase with time. Under these conditions, NOM deposition and permeate flux decline occurred rapidly and each test was completed within 24 hours.

4.3.2 Bench-Scale Tests

An Osmonics SEPA CF membrane cell was used to conduct the bench-scale filtration tests. The membrane cell consists of two rectangular acrylic blocks which are used to sandwich a 155-cm^2, flat-sheet membrane specimen between the feed spacer and permeate carrier. Pressure was applied to the blocks by a piston via compressed air while feedwater was forced through the sealed membrane test cell using a variable speed pump. The feedwater flowed across the flat membrane surface to simulate the crossflow dynamics within spiral wound elements. The total run time for each bench-scale membrane test was two weeks. A schematic of the bench-scale test apparatus is shown in Figure 4-2.

4.3.3 Pilot-Scale Tests

The pilot-scale tests utilized standard 2.5 in. x 40 in. spiral wound membrane elements within standard pressure vessels. The total run time for each pilot-scale membrane test was three weeks. A schematic of the pilot-scale test apparatus is shown in Figure 4-3.

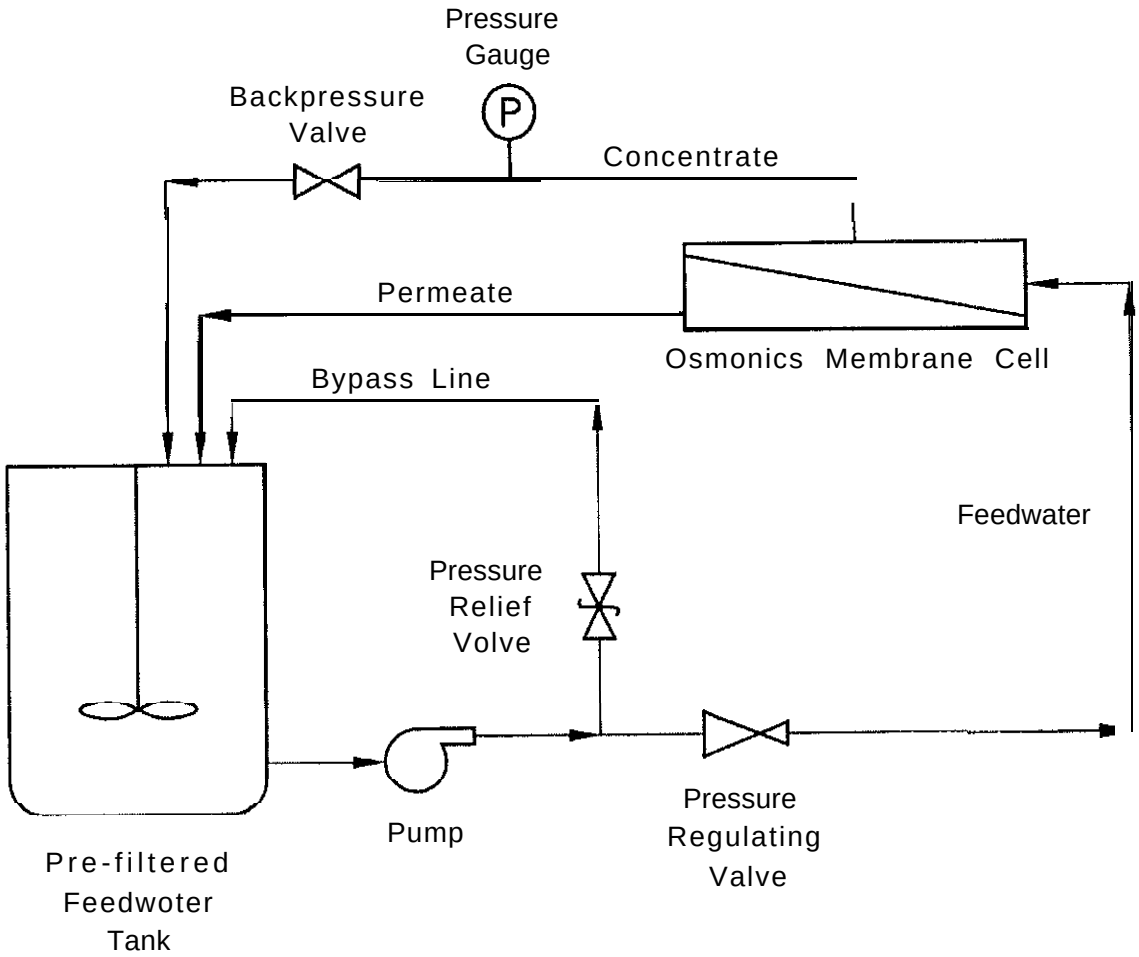

Figure 4.2 - Flow Schematic for Bench Tests

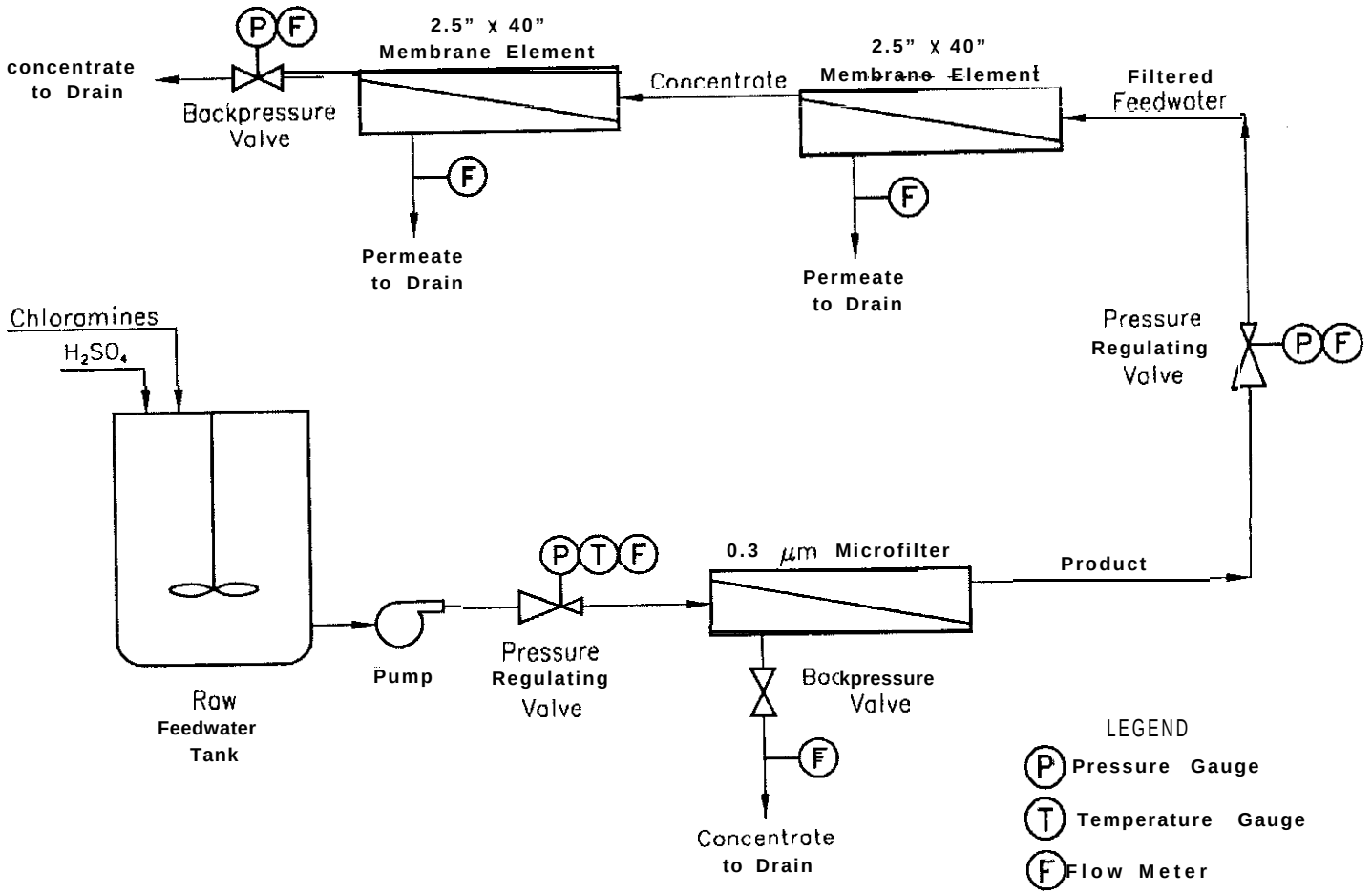

Figure 4.3 - Flow Schematic for Pilot Tests

4.4 Testing Protocol

The **two** source **waters** and two membranes provided a total of four water-membrane combinations. The four water-membrane combinations were tested at each of the three scales of operations and are listed below:

- **EC:** ESNA membrane with CR water
- GC: GM membrane with CR water
- EH: ESNA membrane with HR water
- GH: GM membrane with HR water

The testing protocol was nearly the same for all three scales of testing. Operating parameters for the membrane tests were set within the ranges specified by the membrane manufacturers. The testing protocol and operating parameters are described in the following sections.

4.4.1 Net Driving Pressure

Membrane tests were conducted under constant pressure to observe flux decline due to NOM fouling. For all tests using the ESNA nanofiltration membrane the applied pressure was 70 psi (483 kPa). For all tests using the GM ultrafiltration membrane, the applied pressure was 50 psi (345 kPa). For pilot-scale tests, the actual applied pressure varied ± 15% of the target pressure due to operational/equipment limitations.

Rejection of dissolved solids produced an osmotic pressure differential across the membrane opposite in direction to the applied pressure. The osmotic pressure differential was estimated using the empirical correlations below (Ho and Sirkar, 1992).

$$TDS \approx 0.431\left[\left(1 + 0.00438\sqrt{C}\right)C^{1.02}\right] \tag{4.1}$$

$$\Delta\pi \approx 0.01\left(TDS_f - TDS_p\right) \tag{4.2}$$

where: c = conductivity, µS/cm

$\Delta\pi$ = osmotic pressure differential, psi

TDS, = average TDS of feedwater, mg/L

TDS, = average TDS of permeate, mg/L

The osmotic pressure was negligible for all tests using the GM ultrafiltration membrane due to its low salt rejection. For all tests using the ESNA nanofiltration membrane, the osmotic pressure was less than 3 psi, with the (exception of the stirred cell test using CR water. For this test, dead.-end filtration resulted in a substantial increase in osmotic pressure due to the high TDS concentration of the feedwater and the high salt rejection of the ESNA membrane. The osmotic pressure for the EC test was estimated by a mass balance of TDS using the 85% salt rejection specified by the

manufacturer. The estimated osmotic pressure was subtracted from the applied pressure to yield the net driving pressure for each data point.

The applied pressure was taken as the feedwater inlet pressure for the stirred cell and bench-scale tests. The applied pressure for pilot-scale tests was estimated as the average of the feedwater inlet and concentrate outlet pressures. The permeate stream exited to atmospheric pressure for all three scales of operation.

4.4.2 Feedwater Flow Rate

The research objective of evaluating NOM-membrane interactions in terms of their respective properties at different scales of operation requires hydrodynamic similitude between each scale of operation. Variations in hydrodynamics at the membrane surface were minimized by maintaining the same, constant feedwater velocity for **all** tests. For bench- **and pilot-scale** tests, the feedwater flow rate was set to achieve a crossflow velocity of 20 cm/s. The corresponding feedwater flow rates were calculated as follows:

$$Q_f = v A_{eff} \tag{4.3}$$

$$A_{eff} = w h_{eff} \tag{4.4}$$

where: Q_f = feedwater flow rate, cm^3/s

v = crossflow velocity, 20 cm/s

A_{eff} = effective cross-sectional area, cm^2

w = width of active membrane, cm

h_{eff} = effective channel height, cm

The effective channel height, h_{eff}, was calculated as the spacer thickness multiplied by the porosity of the spacer.

The hydrodynamics at the membrane surface are significantly different for the stirred cell test apparatus because it operates in a dead-end filtration mode, i.e., the feedwater flow rate is equal to the permeate flow rate. For these tests, Q_f was set to a value that provided a flux rate similar to the flux rates observed at the bench- and pilot-scale tests.

Crossflow conditions were simulated by stirring the cell contents with a rotating magnetic stir bar. The speed of stirring has a significant effect on the mass transfer coefficient which influences the development of the concentration-polarization and gel layers. A recent study of nanotiltration using stirred and unstirred cells (Schafer, et al., 1998) found that the mass transfer coefficients varied from 0.14 E-6 ms^{-1} at 0 rpm to 2.18 E-6 ms^{-1} at 560 rpm. The current study employed a stirring speed of 300 rpm for all stirred cell tests to meet the objective of consistency between tests and to

achieve a relatively high flow rate across the membrane surface. No attempt was made to correlate stirring speed with the crossflow hydrodynamics utilized in the bench- and pilot-scale tests. The feedwater flow rates for each scale of testing were:

- Laboratory stirred cell, $Q_f \approx 2.0 \times 10^{-3}$ Umin
- Bench scale, Q, $\approx 7.0 \times 10^{-1}$ Umin
- Pilot scale, $Q_f \approx 1.1$ x IO' L/min

The actual feedwater flow rates varied ± 15% of the target rates due to operational/equipment limitations (especially at the pilot scale). Flow rates were regulated using the pumps and valves shown on the flow schematics (Figure 4-1, 4-2, and 4-3).

4.4.3 initial Clean Water Flux

Prior to commencing each test, deionized water was introduced at the pressure and flow rate specified above to determine the initial permeate flux rate of the clean membrane (i.e., clean water permeability). Flux rates observed thereafter during the test were compared to the initial flux rate to determine the rate of NOM fouling of the membrane surface.

The flux rate of a membrane is greatest when it is first put into operation. The virgin membrane undergoes a process referred to as "setting" or "compression" during the initial hours of operation in which the flux rate gradually decreases and approaches a steady-state value. The amount of time required for completion of the setting process varies with the type of membrane and the applied pressure. Protocol for bench-scale membrane tests pursuant to the ICR (U.S. Environmental Protection Agency, 1996b) recommends initial membrane operation with "...laboratory clean water until the change in the MTC, (mass transfer coefficient of water) over a 12 hour period is less than 4%."

The current study observed clean water flux rates for the ESNA and GM membranes prior to each test for a period between 3 to 10 hours. It was determined that no significant flux decline occurred after a period of about 3 hours. Similar results were obtained in a recent study using the same membranes (Cho, 1998).

Clean-water flux rates were evaluated only at the pressures specified for testing using the source waters (i.e., 70 and 50 psi for the ESNA and GM membranes, respectively). The clean-water flux rates subsequent to setting were used to calculate the hydraulic resistance of each membrane. These membranes were then used for testing with the source waters to observe the change in resistance due to gel layer formation. Completion of the

membrane setting process was required to be able to distinguish between the hydraulic membrane and gel layer resistances. Clean water flux data for each of the tests conducted (see Appendix) indicate that setting was complete prior to testing with the source waters.

5.0 DEVELOPMENT OF GEL RESISTANCE MODEL

One of the primary objectives of this research was to develop a resistance model for NOM fouling of water treatment membranes. There were two principal reasons for developing the model:

1) A fouling model would provide a practical tool for predicting permeate flux decline at larger scales of operation. The results of bench- and pilot-scale tests are normally used to predict performance at larger scales of operation. A flux-decline model that is easy to use could assist the effort to extrapolate test data. Ease of use requires simplifying assumptions to reduce the quantity and complexity of the numerous parameters that affect flux decline.

2) A fouling model would provide a better understanding of the NOM-membrane interactions which influence NOM fouling. Interactions between the NOM and membrane depend on properties of the NOM, feedwater, and membrane. A resistance model that quantitatively incorporates these properties would extend the body of knowledge in this area.

5.1 Resistance to Permeate Flow

Feedwater that permeates the membrane encounters several types of resistance to flow. For this reason, pressure is applied to the system to overcome this resistance and force the water through the membrane. The relationship between permeate flux, resistance, and applied pressure is described by the series resistance equation:

$$J = \frac{AP - An}{\mu\left(R_m + R_g\right)} \qquad (5.1)$$

where:
- J = permeate flux rate (LT^{-1})
- ΔP = applied transmembrane pressure ($ML^{-1}T^{-2}$)
- $\Delta\pi$ = osmotic transmembrane pressure ($ML^{-1}T^{-2}$)
- μ = absolute viscosity of feedwater ($ML^{-1}T^{-1}$)
- R_m = hydraulic resistance of clean membrane (L^{-1})
- R_g = gel resistance on membrane surface (L^{-1})

5.1.1 Osmotic Pressure

Membrane rejection of solutes in the feedwater creates a concentration gradient across the membrane; i.e., the concentration of solutes in the feedwater is usually much greater than the concentration of solutes in the permeate. This concentration gradient creates an osmotic pressure that is opposite in direction to the applied pressure as indicated in

Eq. (5.1). This phenomenon is sometimes interpreted as a resistance to permeate flow and is commonly referred to as the concentration-polarization resistance. An alternative form of Eq. (5.1) is to substitute a concentration-polarization term (i.e., R,,) in the denominator for the osmotic pressure term (An) in the numerator.

5.1.2 Gel Layer Resistance

Dissolved NOM (i.e., < 0.45 µm in size) in the feedwater is carried to the membrane surface by the advective flow of water that permeates the membrane. Some portion of the dissolved NOM also permeates through the membrane and is carried away in the product water. The remainder of the NOM is rejected by the membrane and is either carried back into the bulk feedwater or is adsorbed to the membrane surface. The adsorbed NOM is referred to as the gel layer. The NOM deposit imparts a resistance to the flow of water through the membrane which is referred to as gel resistance, R,. The gel resistance varies directly with the mass of NOM in the gel layer. 'Therefore, gel resistance can be described in terms of the density and thickness of the gel layer.

Adsorption of NOM to the membrane surface is sometimes described as having reversible and irreversible components (i.e., $R_g = R_{rev} + R_{ir}$). The reversible component refers to adsorbed NOM that can be removed by a

cleaning procedure. Adsorbed NOM that is not removed through cleaning is the irreversible component of the NOM gel layer. The amount of adsorbed NOM that can be removed, however, is highly dependent on the cleaning strategy that is employed (i.e., cleaning duration and frequency, cleaning chemicals, temperature, flow rate, etc.) and was not considered in the theoretical development of this gel resistance model.

5.1.3 Hydraulic Resistance of Clean Membrane

The membrane itself imparts a resistance to the flow of water through the membrane. The amount of resistance depends on the quantity and size of the membrane pores. As membrane porosity increases, the resistance to flow decreases. This resistance is referred to as the hydraulic resistance of the clean membrane.

5.1.4 Application of the Series Resistance Equation

Membrane operation can be evaluated using the series resistance equation (5.1) (Wiesner and Aptel, 1996; Bowen and Jenner, 1995). The permeate flux rate, J, and the applied transmembrane pressure, AP, can be directly measured. Osmotic pressure, An, can be measured directly in the laboratory or approximated by an empirical correlation with the concentrations of solute in the feedwater and permeate. The absolute viscosity of the

feedwater,, μ, can be approximated using an empirical correlation with the temperature of the feedwater.

The hydraulic resistance of the clean membrane, R_m, is a constant and can be calculated using Eq. (5.1) by using deionized feedwater and a virgin membrane because under these conditions, $\Delta\pi = R_g = 0$. Once R_m is known, the only remaining unknown in Eq. (5.1) is the gel resistance. During membrane operation, R_g can be calculated using Eq. (5.1) at different points in time by measuring or calculating the other parameters as described above. The primary goal of this research was to develop a model of gel resistance based on NOM-membrane interactions to correlate with the R_g values derived from Eq. (5.1).

Eq. (5.1) predicts that permeate flux increases with increasing transmembrane pressure. In practice, permeate flux is sometimes limited by mass transfer of the solute at the membrane surface. Under conditions of significant high transmembrane pressure and gel resistance, increases in transmembrane pressure are countered by increases in the gel layer resistance. Development of a model for the gel resistance, R_g, provides the flexibility of using Eq. (5.1) under conditions of either pressure-dependent or mass-transfer-limited permeate flux.

5.2 NOM Transport

Development of a gel resistance model requires consideration of the dynamics associated with gel formation. Gel layer formation is a function of NOM transport to and from the membrane surface. There are three primary modes of NOM transport as depicted in Figure 5-1 (concentration-polarization boundaries are neglected).

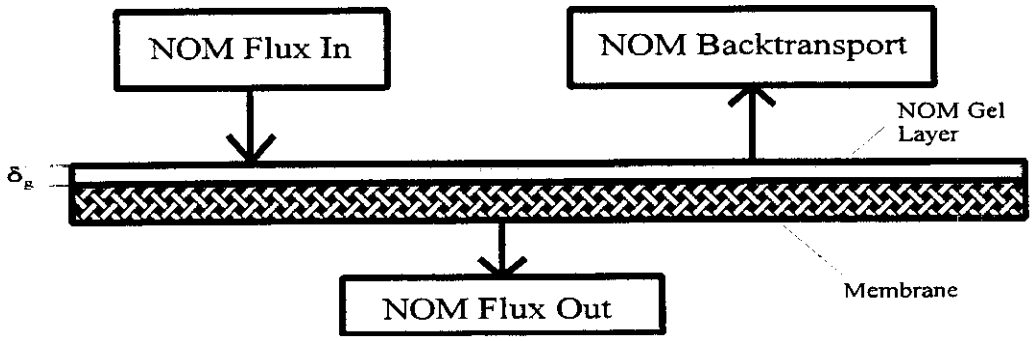

Figure 5.1 NOM Transport at the Membrane Surface

5.2.1 Flux Transport

NOM is carried to and from the membrane surface by the advective permeate flow. The NOM is transported at a rate equal to the permeate flux rate. The mass of NOM carried to and from the membrane surface by permeate advection depends on the concentration of NOM in the bulk feedwater and permeate, respectively. The corresponding mass flux rates of NOM as shown in Fig. 5.1 are:

$$NOM\ Flux\ In = JC_b \quad (5.2)$$

$$NOM\ Flux\ Out = JC_p \quad (5.3)$$

where: C_b = concentration of NOM in bulk feedwater (ML^{-3})

C_p = concentration of NOM in permeate (ML^{-3})

The units of the mass flux terms are mass per unit area of membrane per unit of time ($ML^{-2}T^{-1}$).

5.2.2 Backtransport

NOM that accumulates at the membrane surface is subject to backtransport to the bulk feedwater. NOM backtransport occurs through a combination of advection and diffusion processes (Wiesner and Chellam, 1992). Advective backtransport is strongly influenced by the velocity of the feedwater across the membrane surface (crossflow velocity). Increasing crossflow velocity provides greater inertial lift to NOM deposits allowing them to overcome permeate drag (advection towards the membrane) and be transported back to the bulk feedwater. The amount of inertial lift required depends on NOM-membrane interactions.

Diffusive backtransport is strongly influenced by the NOM concentration gradient between the membrane surface and the bulk

feedwater. Increasing the NOM concentration gradient results in greater diffusive backtransport. The rate of diffusion also depends on NOM-membrane interactions. Based on the above discussion, it follows that:

$$\text{Backtransport} = f(v, \text{A C, NOM-membrane interactions}) \qquad (5.4)$$

where: v = crossflow velocity of feedwater

ΔC = concentration gradient between membrane and bulk feedwater

The objectives of this study were to evaluate NOM fouling in terms of NOM-membrane interactions. Therefore, the research approach was to minimize the influence of other variables such as the crossflow velocity and NOM concentration gradient. The bench- and pilot-scale studies utilized the same crossflow velocity for all tests, 20 cm/s. A rotating stir bar was used in the stirred cell tests to simulate the crossflow hydrodynamics.

Differences in the NOM concentration gradient between the membrane surface and the bulk feedwater also were minimized between the tests. This was accomplished by selecting source waters having nearly the same NOM concentration and by minimizing the development of a concentration-polarization layer.

Under these test conditions it is assumed that differences in NOM backtransport are primarily a function of differences in NOM-membrane interactions between each of the four water-membrane combinations. For modeling purposes, Eq. (5.4) is rewritten as:

$$\text{Backtransport} = f(\text{NOM - membrane interactions}) \tag{5.5}$$

NOM-membrane interactions are expected to decrease with increasing accumulation of NOM mass on the membrane surface. If it is assumed that NOM density is constant over the thickness of the gel layer, and that NOM-membrane interactions are directly proportional to the amount of NOM mass on the membrane surface, then backtransport can be modeled as:

$$\text{Backtransport} = \lambda \delta_g \rho_g \tag{5.6}$$

where: A= backtransporl rate coefficient (T^{-1})

δ_g = thickness of gel layer (L)

ρ_g = density of NOM in gel layer (ML^{-3})

The backtransport rate coefficient, λ, represents the combined effects of all NOM-membrane interactions on the rate of backtransport. The value of A is a constant for each membrane-source water combination. Equation (5.6) indicates that backtransport increases with increasing accumulation of NOM

mass in the gel layer. The units of backtransport are mass per unit area of membrane per unit of time (ML?).

5.3 NOM Mass Balance at the Membrane Surface

Gel resistance is directly proportional to the mass of NOM in the gel layer. The quantity of NOM mass is determined by applying a mass balance to the transport mechanisms defined above and shown in Figure 5.1. As explained previously, the membrane experiments were conducted such that concentration-polarization effects were negligible. Therefore, the control volume for the mass balance is bounded by the gel layer surface and the permeate surface of the membrane. A NOM mass balance at the membrane surface is described by the following equations:

$$\rho_g \frac{d\delta_g}{dt} = \text{NOM Flux In-NOM Flux Out - Backtransport} \qquad (5.7)$$

By substitution:

$$\rho_g \frac{d\delta_g}{dt} = JC_b - JC_p - \rho_g \lambda \delta_g \qquad (5.8)$$

The rate of NOM mass accumulation in the gel layer per unit area of membrane surface ($ML^{-2}T^{-1}$) is described by the left-hand side of Eq. (5.8). The right-hand side is comprised of the NOM transport terms defined above.

53.1 NOM Mass Loading Concept

The difference of the NOM mass flux terms (JC, - JC,) can be interpreted as the NOM mass loading at the membrane surface. Viewed in this manner, the NOM mass loading function is defined:

$$W(t) = J\left(C_b - C_p \right) \tag{5.9}$$

where: W(t) = NOM mass loading function ($ML^{-2}T^{-1}$)

Substitution into Eq. (5.8) and rearrangement of terms yields:

$$\frac{d\delta_g}{dt} + \lambda \delta_g = \frac{W(t)}{\rho_g} \tag{5.19}$$

Equation (5.10) is a first-order, nonhomogeneous, ordinary, linear differential equation. Particular solutions exist for particular forms of the loading function, W(t) (Chapra, 1997). The loading functions encountered in the three scales of membrane operation that were used in this study along with the corresponding particular solutions to Eq. (5.10) are explained in the following sections.

5.4 Gel Resistance Model for Stirred Cell Tests

Dead-end filtration of the feedwater in the stirred cell test apparatus (refer to Figure 4-l) causes the rejected NOM to be returned to and mixed

with incoming feedwater. Gel layer formation on the membrane surface results in permeate flux decline through time. Likewise, the reduced flux rate results in a lower rate of NOM rejection. Consequently, the NOM mass loading function for stirred cell tests is approximately linear with time:

$$W(t) = J\left(C_b - C_p\right) = \beta t \qquad (5.11)$$

where: β = slope of the mass loading function ($ML^{-2}T^{-2}$)

The particular solution to Eq. (5.10) for a linear mass loading function is (Chapra, 1997):

$$\delta_g = \frac{\beta}{\lambda \rho_g}\left(t - \frac{1}{\lambda} + \frac{e^{-\lambda t}}{\lambda}\right) \qquad (5.12)$$

The sum of the λ terms within the parenthesis is quite small and approaches zero rapidly (within 1 hour) after commencing the stirred cell test. For modeling purposes, Eq. (5.12) is reduced to the following simplified form:

$$\delta_g = \frac{\beta}{\lambda \rho_g} t \qquad (5.13)$$

Based on the previous model assumptions that gel resistance varies directly with the mass of NOM in gel layer, and that NOM density is constant over the thickness of the gel layer, gel resistance is related to the thickness of

the gel layer by the following equation:

$$R_g = \epsilon \delta_g \qquad \textit{(5.14)}$$

where: ϵ = specific resistance of the gel layer (L^{-2})

Substitution of Eq. (5.14) into Eq. (5.13) yields the gel resistance model for stirred cell tests:

$$R_g = \frac{\varepsilon}{\lambda \rho_g} \beta t = K \beta t \qquad (5.15)$$

where: K = NOM accumulation coefficient (LTM")

The parameters ϵ, λ, and ρ_g are all constants related to properties of the NOM, membrane, and feedwater. These constants are thus combined into a single rate constant, K, which reflects the aggregate influence of these properties. The aggregate constant, K, represents the fraction of NOM loading, β, that accumulates in the gel layer. Equation (5.15) predicts that gel resistance increases linearly with time.

5.5 Gel Resistance Model for Bench- and Pilot-Scale Tests

Crossflow filtration of feedwater in the bench- and pilot-scale tests

under constant pressure results in permeate flux decline due to NOM fouling. The NOM mass loading function can be approximated as a step input at the beginning of the tests and is described as follows:

$$W(t) = 0 \qquad t < 0 \tag{5.16}$$

$$W(t) = W \qquad t \geq 0 \tag{5.17}$$

where: w = new constant level of loading ($ML^{-2}T^{-1}$)

The particular solution to Eq. (5.10) for a step mass loading function is (O'Neil, 1991):

$$\delta_g = \frac{W}{\lambda \rho_g}\left(1 - e^{-\lambda t}\right) \tag{5.18}$$

Substitution of Eq. (5.14) into Eq. (5.18) yields the gel resistance model for bench- and pilot-scale tests:

$$R_g = \frac{\varepsilon}{\lambda \rho_g} W\left(1 - e^{-\lambda t}\right) = KW\left(1 - e^{-\lambda t}\right) = R_{\max}\left(1 - e^{-\lambda t}\right) \tag{5.19}$$

In similar fashion to the stirred cell model, the NOM accumulation coeffkient, K, represents the fraction of NOM loading, W, that accumulates in the gel layer. Equation (5.19) predicts that gel resistance increases exponentially with time and approaches a steady-state value that can be

considered the maximum gel resistance, R_{max}, under the imposed test conditions.

6.0 EXPERIMENTAL AND MODELING RESULTS

A total of 12 membrane filtration tests were conducted; one test for each of the four water-membrane combinations at each of the three scales of operation. Data collected from these tests were used to calculate gel resistance values through time using the series resistance equation (5.1). The gel resistance, R_g, and the NOM loading function, W(t), for each test were used to calculate the NOM fouling parameters (A and K) for the gel resistance model, Eqs. (5.15) and (5.19). Lastly, the NOM fouling parameters were interpreted in terms of the measured properties of the feedwaters, NOM, and membranes.

Properties of the feedwater, NOM, and membrane influence gel layer formation. NOM accumulates at the membrane surface primarily through physical adsorption. Adsorption is defined as the increase in concentration of a particular component at the surface or interface between two phases (Faust and Aly, 1998). Adsorption processes may be classified as physical or chemical, depending on the nature of the forces involved.

Physical adsorption on solids is attributed to forces of interactions between the solid surface and adsorbate molecules. These interaction forces are termed dispersion forces and are electrostatic in origin. For NOM-

membrane interactions, the dispersion forces are a function of the electrostatic and hydrophobic properties of the feedwater, NOM, and membrane. Additionally, the size and quantity of NOM macromolecules and membrane pore size are factors which affect adsorption.

6.1 Properties of the Feedwater, NOM, and Membranes

Properties of the feedwaters and their dissolved NOM were measured using the methods described in Section 4.1.2. The results are summarized in Table 6.1.

Table 6.1 Properties of Feedwaters and NOM

Source	pH	Conductivity (µS/cm)	DOC (mg/L)	SUVA ($m^{-1}mg^{-1}L$)	Humic Fraction (%)	MW_{NOM} (daltons)
HT	6.7	60	2.8	2.8	38	1100
CR	7.0	1200	3.1	2.0	41	1000

Properties of the membranes were measured using the methods described in Section 4.2.1. The results are summarized in Table 6.2

Table 6.2 Membrane Properties

Membrane	MWCO* (Daltons)	Zeta Potential** (mV)	Contact Angle (degrees)
ESNA	200	-13	60
GM	8000	-17	55

*Provided by membrane manufacturer.
**Measured at pH = 7.0, using KCl electrolyte with C = 10 µS/cm.

6.1.1 Electrostatic Properties

Electrostatic interactions occur primarily between the negatively-charged membrane surface and the negatively-charged constituents of NOM (Le., the humic fraction). The electrostatic repulsion between them inhibits NOM adsorption to the membrane surface. This electrostatic repulsion can be reduced or eliminated by the presence of positively charged ions in the feedwater. Positively charged ions are attracted to the negatively charged NOM in the 'Stern layer." Brownian diffusion causes these positive counterions to be distributed out into the bulk solution in the "diffuse double layer."

An increase of concentration of the positively charged counterions in the bulk feedwater leads to a corresponding increase in the concentration of counterions near the NOM's surface resulting in compression of the double layer. Positively charged ions also complex with the negatively charged NOM. The net effect of double layer compression and complexation is to reduce the electrostatic repulsion between the NOM and membrane, and enhance the adsorption of NOM into the gel layer.

Electrostatic properties of the feedwater are characterized by the pH and conductivity. The pH is a measure of the concentration of negatively-charged hydroxyl ions and positively-charged hydronium ions. At low pH the

predominance of positively-charged hydronium ions reduces the charge density of humic/fulvic acids and the zeta potential of the membrane resulting in a net reduction of electrostatic repulsion between the NOM and membrane. The difference in pH between the HT and CR waters (6.7 and 7.0, respectively) is considered insignificant with respect to its influence electrostatic interactions.

Measurements of conductivity indicate a very large difference in the concentration of dissolved electrolytes between HT and CR waters (60 and 1200 µS/cm, respectively). The much higher concentration of positively-charged ions in the CR water results in a much lower electrostatic repulsion between the CR NOM and membrane as compared to HT water.

The zeta potentials of the membrane surfaces were measured at a pH of 7.0. The difference in zeta potentials between ESNA and GM membranes (-13 and -17 mV, respectively) does not reflect a significant difference in the surface charge.

Of the three electrostatic parameters measured (pH, conductivity, and zeta potential), only the difference in ionic strength was considered significant enough to noticeably impact the degree of gel layer formation. It was expected that the higher ionic strength of the CR water would result in a greater gel resistance as compared to the HT water.

6.1.2 Hydrophobic Properties

The hydrophobic character of the NOM and membrane have an influence on the process of solvation. Hydrophilic NOM has an affinity for the water solvent and is stabilized by the formation of adherent thick layers of water molecules around the NOM. In contrast, hydrophobic NOM has a much lower affinity for water with a corresponding greater potential to come out of solution as a precipitate or to adsorb to a hydrophobic surface.

The degree of NOM hydrophobicity can be estimated by SUVA measurements. High SUVA values (5 - 6 $m^{-1}mg^{-1}L$) indicate a high proportion of hydrophobic humic acids, whereas low SUVA values (2 - 3 $m^{-1}mg^{-1}L$) are typical for NOM that is hydrophilic in character (Krasner, et al., 1999). The SUVA measurements of HT and CR waters (2.8 and 2.0 $m^{-1}mg^{-1}L$, respectively) indicate that both have relatively hydrophilic NOM.

The relative hydrophobic character of the membranes was determined through measurements of the contact angle between the membrane surface and a drop of water. Smaller contact angles reflect a greater affinity (hydrophilicity) of the membrane for water. The difference in contact angle measurements for the ESNA and GM membranes (60 and 55 degrees, respectively) is relatively small.

Measurements of the hydrophobic parameters of the NOM and membranes revealed only minor differences in their respective properties. It was expected that these differences would not have an observable impact on gel layer formation.

6.1.3 Size and Concentration Properties

The quantity or concentration of NOM macromolecules at the membrane surface is a factor in the quantity of NOM that is incorporated into the gel layer. When NOM-membrane interactions are conducive to adsorption, larger quantities of available NOM result in greater NOM adsorption. The quantity of NOM in the feedwaters was measured as the DOC concentration.

The concentration of NOM near the membrane surface depends on the quantity of NOM in the feedwater and the fraction of that quantity that is rejected by the membrane. Size exclusion is a primary factor in NOM rejection. NOM macromolecules larger than the membrane pores are retained at the membrane surface. DOC measurements indicate that HT and CR waters contain about the same quantity of NOM (2.8 and 3.1 mg/L, respectively). Likewise, there is only a 10% difference in the mass-averaged MW of the NOM (1100 and 1000 daltons for HT and CR waters, respectively). It was expected that the minor differences in NOM

concentration and size would have a negligible impact on the formation of the gel layer.

Size exclusion of NOM macromolecules also depends on the pore size of the membranes. The membrane pore size is measured as the MWCO of the filtration of PEG compounds as described in Section 4.2.1. The ESNA nanofiltration membrane has much lower MWCO than the ultrafiltration GM membrane (200 and 8000 daltons, respectively, per manufacturer). Comparison of the MWCO values with the MW of the NOM indicates that the ESNA membrane should have a much higher rejection of NOM than the GM membrane. Therefore, it was expected that the ESNA membrane would have a corresponding higher concentration and adsorption of NOM at the membrane surface.

6.2 Uncertainty Analysis of Experimental and Modeling Results

Scientific measurements are inherently uncertain. These uncertainties arise from inaccuracies in the methods and equipment used to make the measurement. The uncertainty in the experimental and modeling results of this study were evaluated using two different approaches:

1) Analysis of uncertainty of calculated modeling parameters based on the propagation of uncertainty of direct measurements through the calculations.

2) Statistical analysis of uncertainty by least squares fitting of the experimental data to the resistance model.

6.2.1 Propagation of Uncertainty

When measurements are used to calculate other physical quantities, the uncertainties in the measurements propagate through the calculation and produce uncertainty in the final calculated result. Measurement uncertainties are classified into two groups: random and systematic (Tighe and Pellegrino, 1998). Random uncertainties occur through random variations in the methods and equipment used to make the measurement and are revealed by repeating measurements of the same quantity. These repeated measurements can be analyzed to determine the statistical mean or average value. The uncertainty of each measurement is described by the statistical standard deviation which represents the dispersion of the measurements about their mean value.

The dynamic nature of the membrane tests conducted in this study did not permit repeated measurements of the same quantity for any of the parameters of interest and, therefore, did not permit a rigorous analysis of the propagation of uncertainty. When repeated measurements are not available or when the value of the measured parameter is constantly changing, the random uncertainty cannot be statistically evaluated. Consequently, random

uncertainties were assumed for each type of measurement in order to estimate the propagation of these uncertainties.

Systematic uncertainties result from a consistent flaw or error in the method or equipment used to make the measurement. Errors of this sort affect all measurements in the same way. For example, a stopwatch that is running consistently slow will yield underestimates of the time, and no amount of repetition will reveal this source of error nor quantify the associated uncertainty. Standard laboratory practice is to identify and reduce systematic errors until they are much less than the required precision. This is usually accomplished through periodic calibration of the measuring equipment using standards of known value.

Parameters were measured during membrane tests using a variety of scales, gauges, and meters. For the purpose of this analysis, a systematic uncertainty was assumed for each type of measurement based on the type of equipment and its calibration history. The overall uncertainty in a measurement is a combination of the random and systematic uncertainties and can be expressed using the following equation (Taylor, 1997):

$$\delta x = \sqrt{\left(\delta x_{ran}\right)^2 + \left(\delta x_{sys}\right)^2} \tag{6.1}$$

where: δx = overall uncertainty in the measurement of x

δx_{ran} = random uncertainty in the measurement of x

δx_{sys} = systematic uncertainty in the measurement of x

Membrane tests were conducted for the purpose of collecting laboratory data for use in calculating gel resistance modeling parameters. Laboratory measurements of flow rate (Q), temperature (T), applied pressure (ΔP), and NOM concentration (C_b and C_p) were taken periodically during each test. These measurements were used for calculating the hydraulic membrane resistance (R_m), the gel resistance (R_g), the NOM mass loading (W), and the NOM accumulation coefficient (K). The uncertainty of these calculated values was estimated through an analysis of the propagation of uncertainty of the measured values. Formulas for propagation of uncertainty were used for calculations involving sums, products, and functions of several variables (Taylor, 1997).

6.2.2 Uncertainty Analysis based on Least Squares Fitting

The uncertainty of laboratory measurements that have a linear relationship with another physical variable (e.g., time) can be analyzed by least squares fitting (linear regression). This method was employed here because the gel resistance models are based on a combination of linear and exponential (which can be linearized) relationships with measured

parameters. The uncertainty of the modeled parameters is described by a statistical analysis of how well the data fits the expected linear relationship This, type of analysis may be more appropriate than the propagation of assumed uncertainties because most of the modeling parameters (K, R_{max}, and W) were not calculated but rather derived by the least squares fitting process.

6.3 Laboratory Stirred Cell Results

A stirred cell test was conducted for each of the four water-membrane combinations using the methods and apparatus described in Section 4.3.1. The raw data and calculated parameters are presented in Tables 6.3 - 6.6. Plots of the NOM mass loading function, W(t), and NOM gel resistance, R_g, are shown on Figures 6.1 - 6.8.

Table 6.3 Stirred Ceil Test Data for EH Combination

Permeate Incremental Volume (mL)	Incremental Time (min)	Cumulative Time (hr)	Permeate Flow Rate, Q (mL/min)	Permeate Flux, J (L/m^2hr)	Bulk DOC (mg/L)	Permeate DOC (mg/L)	DOC Rejection %	NOM Mass Loading W(t) (mg C/m^2hr)	NOM Gel Resistance R_g (m^{-1})
deionized H_2O			2.13	42.3					R_m = 4.49E+13
0	0	0	0.00	0.0	3.15				0.00E+00
200	101.1	1.7	1.98	39.3	5.89	0.412	93.0	215	3.45E+12
200	104.0	3.4	1.92	38.2	8.64	0.399	95.4	315	4.83E+12
200	106.2	5.2	1.88	37.4	11.4	0.377	96.7	413	5.88E+12
200	110.1	7.0	1.82	36.1	14.2	0.359	97.5	500	7.74E+12
200	114.4	8.9	1.75	34.7	17.0	0.359	97.9	578	9.80E+12
200	117.5	10.9	1.70	33.8	19.8	0.338	98.3	658	1.13E+13
200	120.3	12.9	1.66	33.0	22.6	0.316	98.6	737	1.26E+13
200	122.1	14.9	1.64	32.6	25.5	0.306	98.8	820	1.35E+13

Table 6.4 Stirred Cell Test Data for GH Combination

Permeate Incremental Volume (mL)	Incremental Time (min)	Cumulative Time (hr)	Permeate Flow Rate, Q (mL/min)	Permeate Flux, J (L/m^2hr)	Bulk DOC (mg/L)	Permeate DOC (mg/L)	DOC Rejection (%)	NOM Mass Loading W(t) (mg C/m^2hr)	NOM Gel Resistance R_g (m^{-1})
deionized H_2O			2.12	42.1					R_m = 4.51E+13
0	0	0	0.00	0.0	3.53				0.00E+00
200	103.3 99.5	3.4 1.7	2.01	39.9	5.73	1.33	76.8	176	2.46E+12
200			1.94	38.5	7.73	1.53	80.2	239	4.28E+12
200	105.7	5.1	1.89	37.6	9.70	1.56	83.9	306	5.42E+12
200	108.2	6.9	1.85	36.7	11.5	1.76	84.7	358	6.62E+12
200	111 1	8.8	1.80	35.8	12.9	2.09	83.8	387	8.00E+12
200	112.5	10.7	1.78	35.3	14.3	2.19	84.7	428	8.67E+12
200	114.9	12.6	1.74	34.6	15.4	2.36	84.7	451	9.82E+12
200	116.6	14.5	1.72	34.:	16.5	2.42	85.3	480	1.06E+13

Table 6.5 Stirred Cell Test Data for EC Combination

Permeate Incremental Volume (mL)	Incremental Time (min)	Cumulative Time (hr)	Permeate Flow Cl	Permeate Rate, (mL/min)	Permeate Flux, J (L/m^2hr)	Bulk DOC (mg/L)	Permeate DOC (mg/L)	DOC Rejection %	NOM Mass Loading W(t) (mg C/m^2hr)	NOM Gel Resistance R_a (m^{-1})
deionized H_2O				2.14	42.5					R_m = 4.46E+13
0	0	0		0.00	0.0	4.80				0.00E+00
200	113.1	1.9		1.77	35.1	8.95	0.652	92.7	292	8.62E+12
200	119.8	3.9		1.67	33.2	13.2	0.513	96.1	421	1.10E+13
200	127.2	6.0		1.57	31.2	17.5	0.486	97.2	532	1.35E+13
200	135.6	8.3		1.47	29.3	21.9	0.483	97.8	628	1.64E+13
200	144.0	10.7		1.39	27.6	26.2	0.501	98.1	709	1.83E+13
200	152.8	13.2		1.31	26.0	30.4	0.531	98.3	777	2.00E+13
200	160.3	15.9		1.25	24.8	34.7	0.578	98.3	846	2.10E+13
200	167.2	18.7		1.20	23.8	38.7	0.748	98.1	902	2.27E+13

Table 6.6 Stirred Cell Test Data for GC Combination

Permeate Incremental Volume (mL)	Incremental Time (min)	Cumulative Time (hr)	Permeate Flow Q	Permeate Rate, (mL/min)	Permeate Flux, J (L/m^2hr)	Bulk DOC (mg/L)	Permeate DOC (mg/L)	DOC Rejection %	NOM Mass Loading W(t) (mg C/m^2hr)	NOM Gel Resistance R_a (m^{-1})
deionized H_2O				2.27	45.1					R_m = 4.21E+13
0	0	0		0.00	0.0	4.78				0.00E+00
200	93.1	1.6		2.15	42.7	6.97	2.59	62.8	187	2.38E+12
200	99.2	3.2		2.02	40.1	8.88	2.87	67.7	241	5.30E+12
200	101.3	4.9		1.97	39.2	10.80	3.04	71.3	297	6.30E+12
200	103.0	6.6		1.94	38.6	12.2	3.22	73.6	347	7.11E+12
200	104.4	8.4		1.92	38.1	13.6	3.35	75.4	390	7.78E+12
200	107.7	iO.I		1.86	36.9	14.8	3.56	75.9	415	9.36E+12
200	109.7	12.0		1.82	36.2	16.0	3.62	77.4	449	1.03E+13
200	111.6	13.8		1.79	35.6	17.0	3.79	77.7	470	1.12E+13

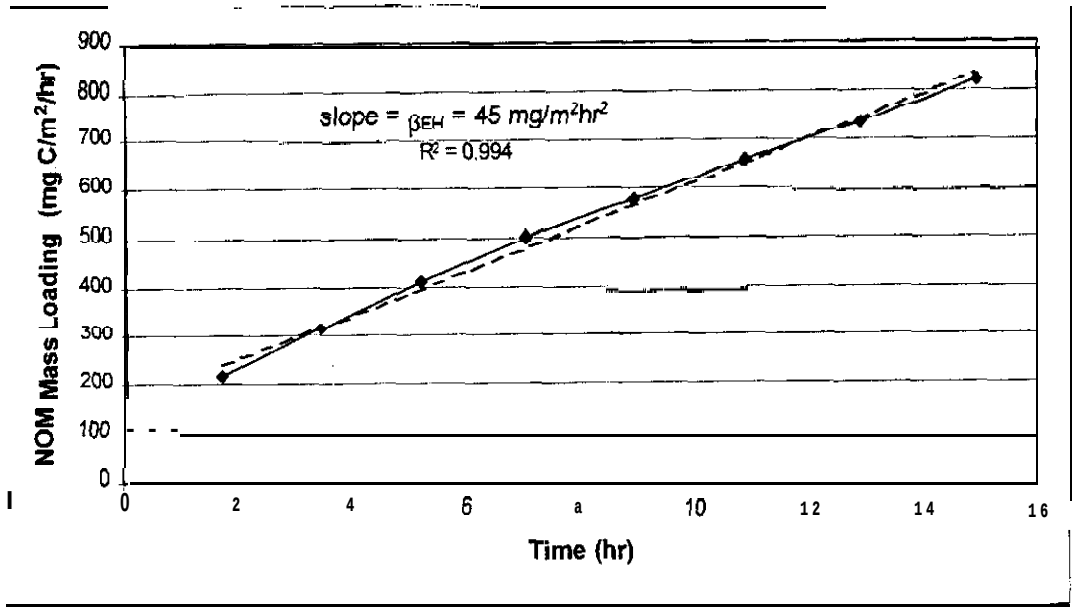

Figure 6.1 NOM Mass Loading for Stirred Cell EH Combination

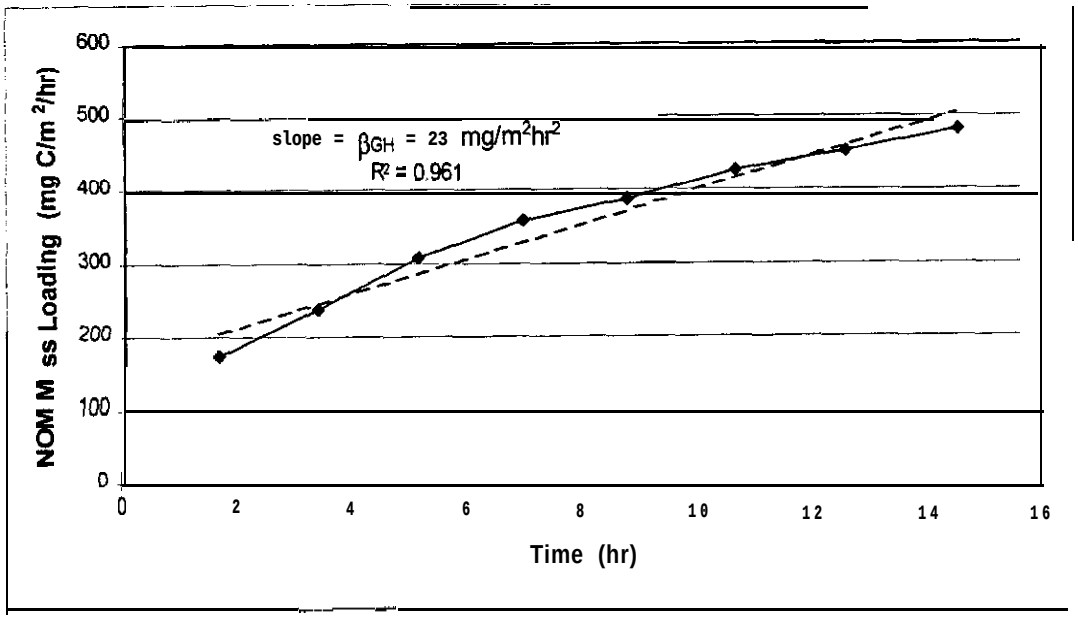

Figure 6.2 NOM Mass Loading for Stirred Cell GH Combination

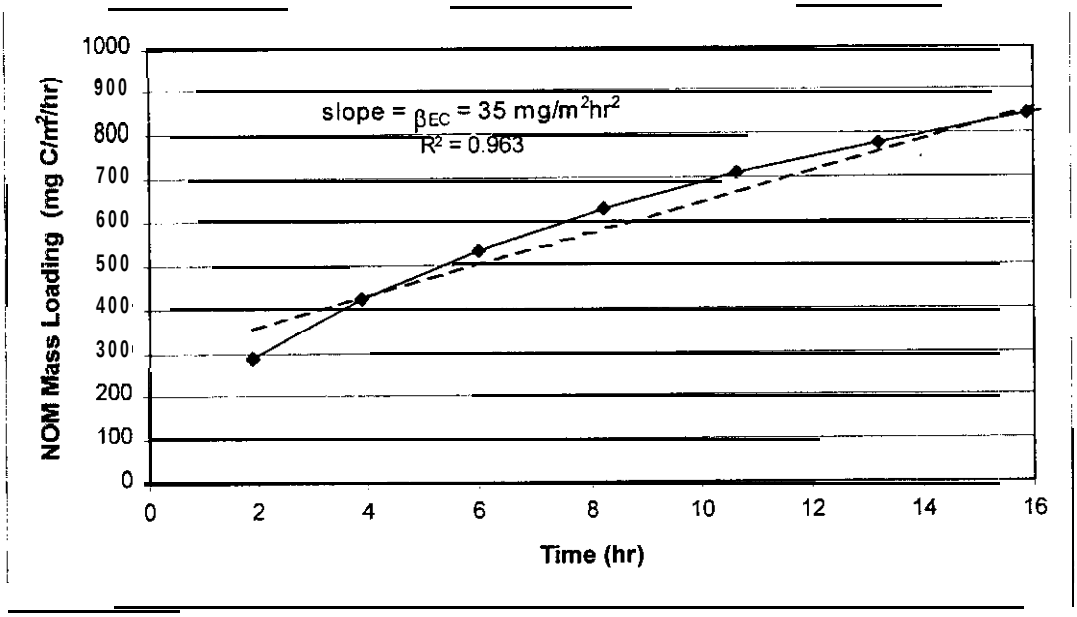

Figure 6.3 NOM Mass Loading for Stirred Cell EC Combination

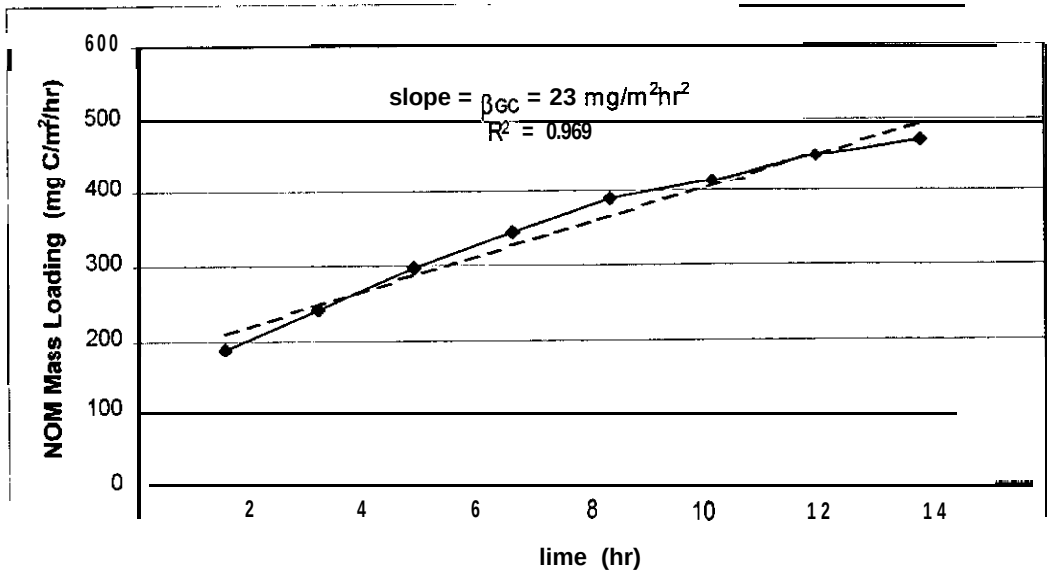

Figure 6.4 NOM Mass Loading for Stirred Cell GC Combination

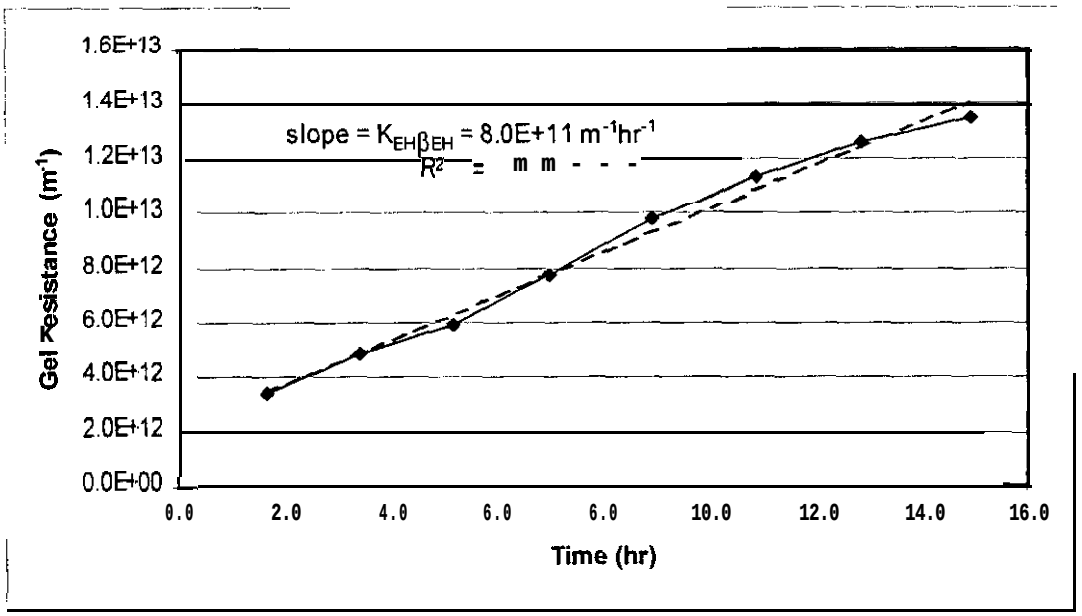

Figure 6.5 NOM Gel Resistance for Stirred Cell EH Combination

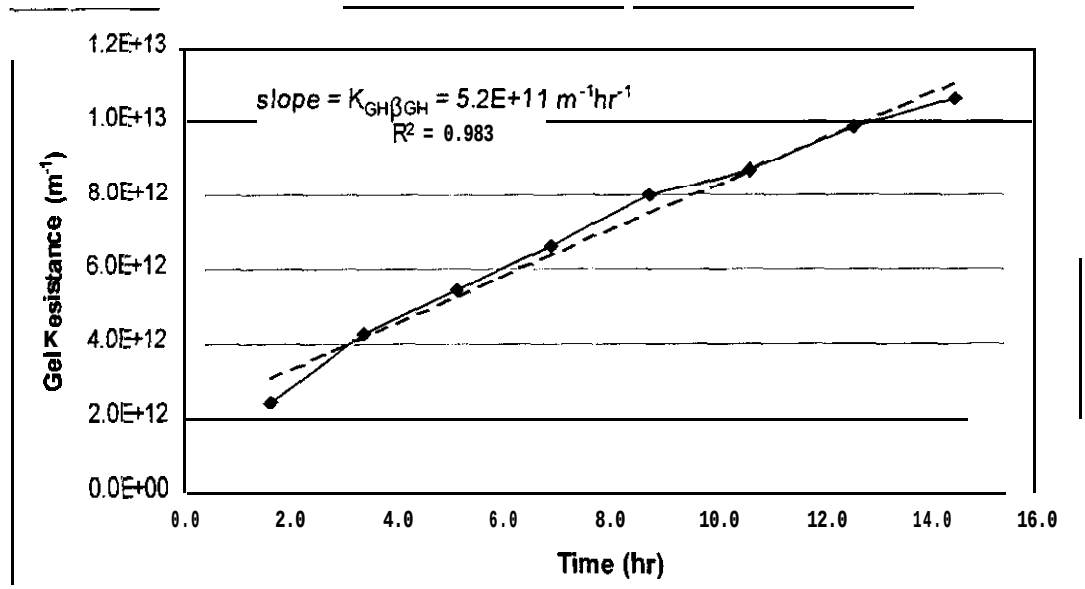

Figure 6.6 NOM Gel Resistance for Stirred Cell GH Combination

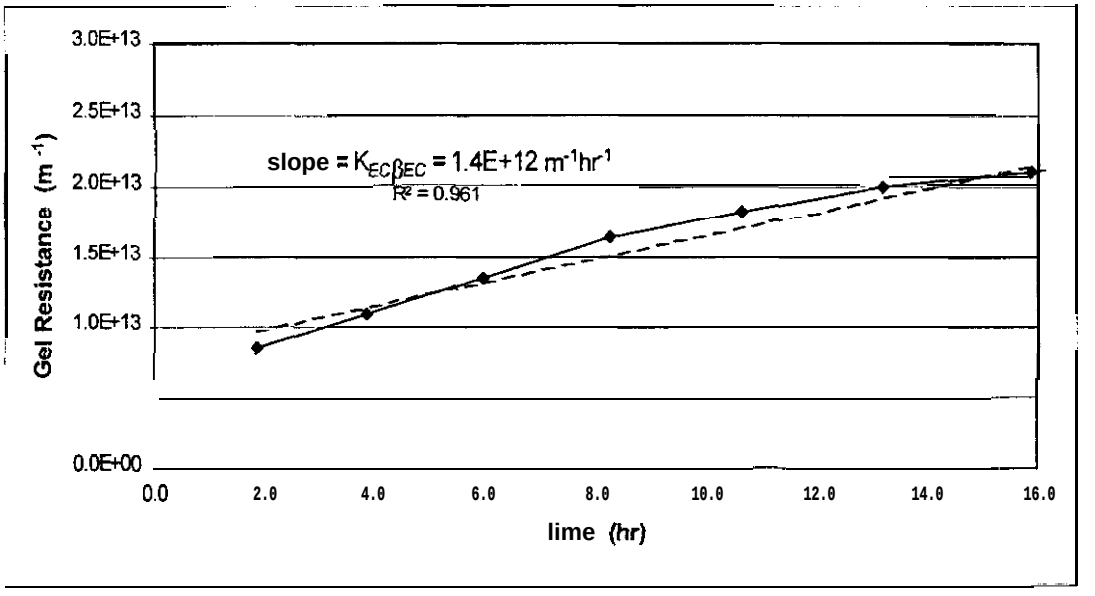

Figure 6.7 NOM Gel Resistance for Stirred Cell EC Combination

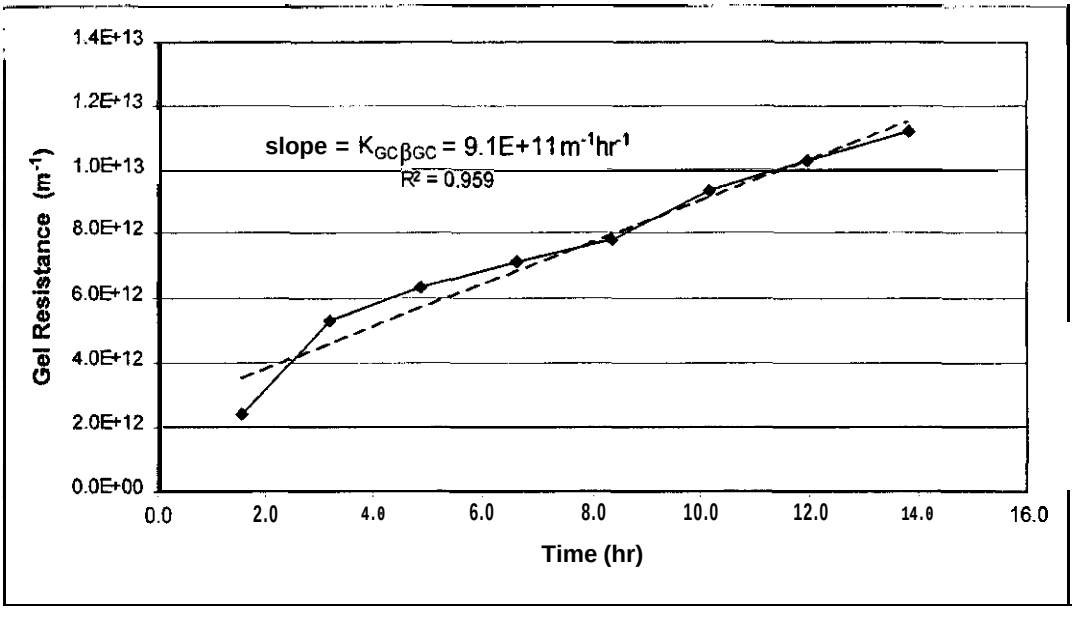

Figure 6.8 NOM Gel Resistance for Stirred Cell GC Combination

6.3.1 Propagation of Uncertainty for Stirred Cell Tests

The propagation of uncertainty for the modeling parameters for the stirred cell tests was determined through an analysis of each of the measured quantities and the intermediate calculations as described in the following sections.

6.3.1.1 Uncertainty of Applied Pressure, ΔP

The applied pressure was measured using a pressure gauge having an accuracy of 3% in the range of pressures that were measured (per manufacturer); this value is taken as the random uncertainty of the measurement. The systematic uncertainty is assumed to be 3 psi. The overall uncertainty of each pressure measurement, ΔP, is calculated as:

$$\mathbf{SAP} = \sqrt{(0.03\Delta P)^2 + (3)^2} \tag{6.2}$$

6.3.1.2 Propagation of Uncertainty for Absolute Viscosity, μ

The absolute viscosity of the feedwater was estimated using the "power law" for deionized water which is an empirical relation having an accuracy of about 1%, (White, 1986):

$$\ln\frac{\mu}{\mu_0} = -1.94 - 4.80\left(\frac{273}{T}\right) + 6.74\left(\frac{273}{T}\right)^2 \tag{6.3}$$

where: μ_0 = absolute viscosity of water at 273K, 0.001792 kg/m•s

T = temperature of feedwater, K

The uncertainty of the calculated absolute viscosity due to the empirical inaccuracy is: $\delta\mu_e = 0.01\mu$.

Additional uncertainties are introduced by the temperature measurements and the difference between the absolute viscosity of deionized water using Eq. (6.3) and the absolute viscosity of the source waters used for testing. The temperature of the feedwater was measured using a mercury thermometer having an accuracy of 1.5 °C (random uncertainty). Additionally, each temperature measurement is assumed to have a systematic uncertainty of 1 .0 "C. Using Eq. (6.1) the total uncertainty in each temperature measurement is calculated as:

$$\delta T = \sqrt{(1.5)^2 + (1.0)^2} = 1.8\,^{\circ}C \tag{6.4}$$

The propagation of uncertainty in the calculation of the absolute viscosity due to the uncertainty of the temperature measurement is calculated using the following equations (Taylor, 1997):

$$\delta\mu_T = \left|\frac{\partial\mu}{\partial T}\right|\delta_T \tag{6.5}$$

$$\frac{\partial \mu}{\partial T} = \mu_0 \left[4.80\left(\frac{273}{T^2}\right) - 2(6.74)\left(\frac{273^2}{T^3}\right) \right] \exp\left[-1.94 - 4.80\left(\frac{273}{T}\right) + 6.74\left(\frac{273}{T}\right)^2 \right] \tag{6.6}$$

Equation (6.3) provides the approximate absolute viscosity for deionized water. The viscosity of water containing 1000 mg/L of salt is about 0.2% greater than salt-free water (Weast, et al., editors, 1990). The corresponding systematic uncertainty of the calculated absolute viscosity due to the presence of dissolved salts in the source waters is: $\delta\mu_s$ = 0.002~. The overall uncertainty of each calculated value of absolute viscosity is given by:

$$\delta \mu = \sqrt{\delta \mu_e^2 + \delta \mu_T^2 + \delta \mu_s^2} \tag{6.7}$$

6.3.1.3 Propagation of Uncertainty for Permeate Flux, J

The permeate flux rate is defined as:

$$J = \frac{Q}{A} \tag{6.8}$$

where: J = permeate flux rate, L/m²•hr

Q = permeate flow rate, Uhr

A = area of membrane, m²

The area of membrane surface is fixed by the test equipment and does not vary between individual tests. The diameter of the disk-shaped

membrane was measured using a ruler as d = 0.062 m with an uncertainty of $\delta d = \pm$ 0.001 m. The uncertainty of the calculated area is expressed using the following equation (Taylor, 1997):

$$\frac{\delta A}{A} = 2\left(\frac{\delta d}{d}\right) \tag{6.9}$$

The uncertainty of the permeate flux rate, J, is dependent on the uncertainty of the permeate flow rate, Q, which was measured using a 500-mL graduated cylinder and a stopwatch. The accuracy of the graduation marks on the graduated cylinder (0.05%, per manufacturer) is negligible compared to the uncertainty introduced by the operator in reading the graduated cylinder and in starting and stopping the watch. Variations in the method of measurement are minimal because the same operator conducted all of the stirred cell tests. The total uncertainty of the measured permeate flow rate is assumed to be 8% of the measured value: δQ = 0.080. The uncertainties in the measurements of membrane area and permeate flow rate are propagated in the calculation of the permeate flux rate by the following equation (adapted from Taylor, 1997):

$$\frac{\delta J}{J} = \sqrt{\left(\frac{\delta Q}{Q}\right)^2 + \left(\frac{\delta A}{A}\right)^2} \tag{6.10}$$

6.3.1.4 Propagation of Uncertainty for Membrane Resistance, R_m

The hydraulic membrane resistance for stirred cell tests was determined using deionized water and a virgin membrane according to the following equation:

$$R_m = \frac{\Delta P}{\mu J} \tag{6.11}$$

The uncertainty of the calculated R_m value results from the propagation of uncertainties in the parameters on the right side of Eq. (6.11) and is expressed as follows (adapted from Taylor, 1997):

$$\frac{\delta R_m}{R_m} = \sqrt{\left(\frac{\delta \Delta P}{\Delta P}\right)^2 + \left(\frac{\delta \mu}{\mu}\right)^2 + \left(\frac{\delta J}{J}\right)^2} \tag{6.12}$$

6.3.1.5 Propagation of Uncertainty for Osmotic Pressure, An

Osmotic pressure, An, in the stirred cell tests occurred only when using the ESNA membrane (An = 0 for tests using the GM membrane). For the ESNA membrane, the osmotic pressure was determined at the beginning of the stirred cell tests (t = 0) by measuring the conductivity of the feedwater and using the empirical correlations Eqs. (4.1) and (4.2). For all points in time thereafter, the osmotic pressure was estimated using a mass balance based on the membrane manufacturer's specification of 85% salt rejection.

Uncertainty in the calculated values of osmotic pressure is introduced through the measurement of the conductivity as well as the inaccuracies of the empirical equations and mass balance. The initial osmotic pressure calculation is assumed to have 10% uncertainty. The osmotic pressure calculations based on the salt mass balance are assumed to add 3% uncertainty over each successive time interval. The uncertainty in the osmotic pressure for the stirred cell tests using the ESNA membrane was calculated at the end of each time interval, i, as follows:

$$\frac{\delta \Delta \pi_i}{\Delta \pi_i} = 0.10 + \sum_{i=0}^{i=n} 0.03i \qquad \textbf{(6.13)}$$

6.3.1.6 Propagation of Uncertainty for Gel Resistance, R_g

The gel resistance for stirred cell tests was calculated using the equation shown below:

$$R_g = \frac{\mathrm{AP} - \Delta \pi}{\mu J} - R_m \qquad \textbf{(6.14)}$$

The uncertainty in the calculated values of R_g results from the propagation of uncertainties in the measured and calculated parameters described in the sections above, and is determined using the following equation (adapted from Taylor, 1997):

$$\delta R_g = \sqrt{\left(\frac{\partial R_g}{\partial J}\delta J\right)^2 + \left(\frac{\partial R_g}{\partial \mu}\delta \mu\right)^2 + \left(\frac{\partial R_g}{\partial \Delta P}\delta \Delta P\right)^2 + \left(\frac{\partial R_g}{\partial \Delta \pi}\delta \Delta \pi\right)^2 + \left(\frac{\partial R_g}{\partial R_m}\delta R_m\right)^2} \quad (6.15)$$

6.3.1.7 Propagation of Uncertainty for NOM Mass Loading, W

The NOM mass loading parameter was defined in Eq. (5.9) in terms of Rux (J) and NOM concentration (C, ~ C,), and is repeated below:

$$W = J(C_b - C_p) \quad (5.9)$$

The accuracy of the NOM concentration measurements was determined to be within 5% over the range of measured values based on calibration measurements using a standard reagent, potassium hydrogen phthalate. The uncertainty of the measured NOM concentration values is written as follows:

$$\frac{\delta C_b}{C_b} = \frac{\delta C_p}{C_p} = 0.05 \quad (6.16)$$

The uncertainty of the calculated values of W is based on the propagation of uncertainties in J, C_b, and C_p, and is calculated as follows:

$$\frac{\delta W}{W} = \sqrt{\left(\frac{\delta J}{J}\right)^2 + \left(\frac{\sqrt{\left(\delta C_b\right)^2 + \left(\delta C_p\right)^2}}{C_b - C_p}\right)^2} \qquad (6.17)$$

6.3.1.8 Propagation of Uncertainty for NOM Accumulation Coefficient, K

The NOM accumulation coefficient for the stirred cell tests is defined as the ratio of the slope of gel resistance to the slope of NOM mass loading:

$$K = \frac{\Delta R_g / \Delta t}{\Delta W / \Delta t} \qquad (6.18)$$

The slopes of gel resistance and NOM mass loading were determined using the graphical plots on Figures 6.1 thru 6.8. Equation (6.19) was solved as the difference between two points near the fitted slopes (i.e., $\Delta Rg = R_{g2} - R_{g1}$, and $\Delta W = W_2 - W$,) over the same time interval (At). The uncertainty of each time measurement is assumed to be: δt = 0.1 hr. The uncertainty in the calculated value of K results from the propagation of uncertainty from two gel resistance calculations, two NOM mass loading calculations, and four time measurements, and can be determined by solving the following series of equations (adapted from Taylor, 1997):

$$\delta \Delta R_g = \sqrt{\left(\delta R_{g_2}\right)^2 + \left(\delta R_{g_1}\right)^2} \qquad (6.19)$$

$$\delta \Delta W = \sqrt{\left(\delta W_2\right)^2 + \left(\delta W_1\right)^2} \tag{6.20}$$

$$\delta \Delta t = \sqrt{\left(\delta t_2\right)^2 + \left(\delta t_1\right)^2} \tag{6.21}$$

$$\frac{\delta\left(\Delta R_g / \Delta t\right)}{\Delta R_g / \Delta t} = \sqrt{\left(\frac{\delta \Delta R_g}{\Delta R_g}\right)^2 + \left(\frac{\delta \Delta t}{\Delta t}\right)^2} \tag{6.22}$$

$$\frac{\delta(\Delta W / \Delta t)}{\Delta W / \Delta t} = \sqrt{\left(\frac{\delta \Delta W}{\Delta W}\right)^2 + \left(\frac{\delta \Delta t}{\Delta t}\right)^2} \tag{6.23}$$

$$\frac{\delta K}{K} = \sqrt{\left(\frac{\delta\left(\Delta R_g / \Delta t\right)}{\Delta R_g / \Delta t}\right)^2 + \left(\frac{\delta(\Delta W / \Delta t)}{\Delta W / \Delta t}\right)^2} \tag{6.24}$$

6.3.2 Least Squares Uncertainty for Stirred Cell Tests

Plots of NOM mass loading, W, vs. time and gel resistance, R_g, vs. time demonstrated the linear relationships derived in the gel resistance model. Least squares fitting was used to estimate the slopes of these lines which were used to calculate the NOM accumulation coefficient, K. The least squares analysis assumed that the uncertainties in the time measurements are insignificant relative to the uncertainties in the calculated values of Wand

R_g. This assumption was validated in the propagation of uncertainty analysis in the previous sections. Uncertainties in the values of Wand R_g were calculated in terms of their standard deviations from their respective least squares fitted lines using the following equation (Taylor, 1997):

$$\sigma_y = \sqrt{\frac{1}{N-2}\sum_{i=1}^{N}\left(y_i - A - Bx_i\right)^2} \qquad (6.25)$$

where: σ_y = uncertainty of parameter y (i.e., Wor R_g)

N = number of data points

y = value of parameter y, (i.e., Wor R_g)

x = value of parameter x, (time)

A = y-intercept of least squares fitted line

B = slope of least squares fitted line

Assuming a normal distribution of uncertainties, about 68% of the calculated parameters (Wand R_g) lie within one standard deviation of the least squares fitted line, and about 95% lie within two standard deviations. The uncertainty of the least squares slope, B, was calculated from the following equation (Taylor, 1997):

$$\sigma_B = \sigma_y \sqrt{\frac{N}{N\sum x^2 - \left(\sum x\right)^2}} \qquad (6.26)$$

The NOM accumulation coefficient, *K,* was calculated as the ratio of the slope of gel resistance vs. time to the slope of NOM mass loading vs. time from their respective least squares fitted lines. The uncertainty of *K* was calculated as follows (adapted from Taylor, 1997):

$$\sigma_K = K\sqrt{\left(\frac{\sigma_\beta}{\beta}\right)^2 + \left(\frac{\sigma_{\Delta R_g/\Delta t}}{\Delta R_g/\Delta t}\right)^2} \qquad (6.27)$$

6.3.3 Discussion of Laboratory Stirred Cell Results

The plots of the NOM mass loading function, W(t), show a linear increase with time for all four source water-membrane combinations. The slopes of these plots provide the β values for the stirred cell resistance model, Eq. (5.15). Similarly, the plots of NOM gel resistance, R_g, increase linearly with time for all four source water-membrane combinations. The slopes of these plots divided by their β values yields the *K* parameters for the stirred cell resistance model, Eq. (5.15). These modeling parameters are summarized in Table 6.7. Higher rates of NOM mass loading (β values) are observed for the ESNA membrane as compared to the GM membrane. This is due to the larger MWCO of the GM membrane which permits greater permeation of the dissolved NOM. The lower β value for the EC test as compared to the EH test is the result of more rapid flux decline using CR water.

Table 6.7 Stirred Cell Modeling Parameters

Test	β (mg/m^2hr^2)	Uncertainty,% Propag. Analysis	Uncertainty,% Least Sq. Analysis[1]	$\Delta R_g/\Delta t$ ($m^{-1}hr^{-2}$)	Uncertainty, % Propag. Analysis	Uncertainty, % Least Sq. Analysis'	K (mhr/mg)	Uncertainty, % Propag. Analysis	Uncertainty, % Least Sq. Analysis'
EH	45	15	2.9	8.0E11	82	4.3	0.18E11	84	2.6
GH	23	21	8.0	5.2E11	110	7.2	0.23E11	120	4.6
EC	35	18	8.0	14Ell	71	5.8	0.40E11	73	4.9
GC	23	22	6.9	9.1E11	120	11	0.40E11	120	6.3

'Percent uncertainty for least squares analysis based on two standard deviations (95% confidence level): % uncertainty = $2\sigma_y/y$.

The NOM accumulation coefficient, K, represents the proportion of the NOM mass loading, β, that is incorporated into the gel layer. The K parameter is comprised of constants that describe properties of the feedwater, NOM, and membrane which influence NOM-membrane interactions. As shown in Table 6.7, the Kvalues for each source water are about the same, however, they differ by a factor of two between the source waters. The larger Kvalues for CR water are attributed to the much greater ionic strength of the CR water. The greater ionic strength reduces the electrostatic repulsion between the NOM and membrane which leads to increased gel resistance. The linear increase of gel resistance with time was predicted by the gel resistance model. Additionally, test data support the theory and definition of the NOM accumulation coefficient, K, for the stirred cell model.

The uncertainty in the modeling parameters was much greater using the propagation analysis as compared to the least squares analysis. The greatest source of uncertainty in the propagation analysis occurred during the calculation of R_g using Eq. (6.14). Specifically, the relatively minor [uncertainties (about 10%) of the hydraulic membrane resistance, R_m, and the total resistance, $R_T = (\Delta P - \Delta \pi)/\mu J$, were greatly magnified when taking their difference because the R_g values were about one order of magnitude smaller than the corresponding values of R_m and R_T. The lower uncertainty values

determined using the least squares fitting is more consistent with the data dispersion that is shown in Figures 6.1 - 6.8. This would suggest that one or more of the assumed uncertainties in the laboratory measurements were too conservative.

6.4 Bench-Scale Results

A bench-scale test was conducted for each of the four source water-membrane combinations using the methods and apparatus described in Section 4.3.2. The raw data and calculated parameters are presented in Tables 6.8 - 6.11. Plots of the NOM mass loading function, W(t), and NOM gel resistance, R_g, are shown on Figures 6.9 - 6.16.

Table 6.6 Bench-Scale Test Data for EH Combination

Time (hr)	Temp. (°C)	Absolute Viscosity μ (Pa*s)	Permeate Flow, Q (mL/min)	Normalized Flux, J L/m²/hr)	Bulk DOC (mg/L)	Permeate DOC (mg/L)	DOC Rejec. (%)	Mass Loading m a	Gel Resist. C/m²hr) (m⁻¹)
Deion. H_2O	25.4	9.02E-04	11.4	43.7					R_m = 4.41E+13
0.3	22.3	9.71E-04	10.1	42.4					5.32E+11
0.7	23.0	9.55E-04	10.1	41.5	2.53	0.17	93.3	98.0	9.82E+11
1.3	23.7	9.39E-04	10.2	41.1					9.49E+11
4.3	26.0	8.90E-04	10.8	40.8					3.94E+12
8.3	25.7	8.76E-04	10.8	39.8					5.74E+12
12.3	27.0	8.70E-04	10.8	39.5	2.55	0.15	94.1	94.7	6.53E+12
22.3	26.5	8.80E-04	10.4	38.8	2.58	0.13	95.0	94.5	7.12E+12
24.3	26.2	8.86E-04	10.4	38.9					6.32E+12
27.3	26.0	8.90E-04	10.2	38.4					6.77E+12
38.3	27.4	8.62E-04	10.4	37.5					9.58E+12
50.3	26.0	8.90E-04	10.0	37.8	2.58	0.10	98.1	92.8	7.79E+12
82.3	26.7	8.76E-04	10.1	37.2					9.19E+12
72.8	25.0	8.90E-04	9.9	37.3	2.98	0.09	97.0	106.9	8.31E+12
85.3	26.5	8.80E-04	10.1	37.4					8.64E+12
95.8	28.4	8.82E-04	9.9	38.8	2.37	0.10	95.8	83.6	9.42E+12
97.3	26.2	8.86E-04	9.9	37.0					8.86E+12
108.8	27.0	8.70E-04	10.1	38.9					1.00E+13
122.3	26.0	8.90E-04	9.8	38.9	1.97	0.09	95.4	89.3	8.85E+12
141.3	28.2	8.86E-04	9.7	36.3	2.18	0.10	95.4	75.5	9.96E+12
145.8	26.2	8.86E-04	9.7	38.3					9.96E+12
155.8	25.6	8.98E-04	9.8	38.8					8.82E+12
171.3	25.0	9.11E-04	9.2	35.7	2.22	0.08	98.4	78.3	9.41E+12
178.3	24.8	9.15E-04	9.2	35.9					8.84E+12
190.3	25.7	8.96E-04	9.4	35.7	2.28	0.09	98.1	78.2	1.02E+13
196.3	25.0	9.11E-04	9.4	38.4					8.27E+12
2043	25.4	9.02E-04	9.4	36.0					9.38E+12
214.3	25.8	8.98E-04	9.4	35.8	2.45	0.09	98.3	84.5	9.95E+12
228.3	24.3	9.26E-04	9.1	38.0	2.33	0.10	95.7	80.3	8.03E+12
239.3	24.3	9.26E-04	9.0	35.8	2.37	0.09	96.2	81.2	8.61E+12
243.3	24.1	9.30E-04	8.9	35.4					8.64E+12
252.3	24.8	9.15E-04	9.2	35.9					8.84E+12
283.8	24.4	9.24E-04	9.0	35.5	2.51	0.18	92.8	82.7	8.89E+12
277.3	25.1	9.09E-04	9.2	35.8					9.69E+12
289.8	24.9	9.13E-04	9.1	35.4	2.53	0.25	90.1	80.7	9.71E+12
297.3	24.6	9.19E-04	9.1	35.7					8.86E+12
312.8	25.5	9.00E-04	9.4	35.9	2.55	0.13	94.9	88.9	9.67E+12
321.8	24.4	9.24E-04	9.0	35.5					8.89E+12
334.8	24.9	9.13E-04	8.9	34.8					1.09E+13

Table 6.9 Bench-Scale Test Data for GH Combination

Time (hr)	Temp. (°C)	Absolute Viscosity μ (Pa's)	Permeate Flow, Q (mL/min)	Normalized Flux, J (L/m²/hr)	Bulk DOC (mg/L)	Permeate DOC (mg/L)	DOC Rejec. (%)	Mass Loading (mg C/m²hr)	Gel Resist. (m^{-1})
Deion. H2O	22.4	9.69E-04	18.6	77.9					R_m = 2.30E+13
0.1	22.4	9.69E-04	18.0	75.3					7.68E+11
0.4	22.6	9.59E-04	17.8	73.6	3.07	1.00	67.4	152	1.56E+12
1.0	23.5	9.43E-04	17.9	72.5					2.35E+12
2.3	24.6	9.19E-04	17.6	69.0					4.33E+12
11.0	25.6	8.98E-04	17.0	64.7	3.12	1.07	65.7	133	6.84E+12
23.0	26.2	8.86E-04	16.9	63.2	3.06	1.05	65.7	127	7.98E+12
27.0	25.6	8.94E-04	16.6	62.8					7.88E+12
36.5	25.6	8.98E-04	16.3	62.1	3.01	1.05	65.1	122	8.12E+12
49.5	26.0	8.90E-04	16.3	61.3					8.78E+12
61.0	25.6	8.94E-04	16.1	60.9	2.99	1.02	65.9	120	8.84E+12
86.0	26.3	8.84E-04	16.0	59.7	2.93	1.00	65.9	115	9.89E+12
89.8	26.0	8.90E-04	15.9	59.8	2.99	1.05	64.9	116	9.58E+12
106.5	26.9	8.72E-04	16.2	59.4	2.94	1.03	65.0	113	1.05E+13
1130.5	26.3	8.84E-04	15.9	59.3	2.95	1.02	65.4	114	1.01E+13
138.8	25.7	8.96E-04	15.5	58.8					9.90E+12
156.1	26.7	8.76E-04	15.6	57.5	3.25	1.06	67.4	126	1.15E+13
158.8	25.9	8.92E-04	15.5	58.5	2.95	1.05	84.4	111	1.03E+13
188.5	25.7	8.96E-04	15.4	58.5	3.06	1.09	64.4	115	1.01E+13
									1.02E+13
201.1	22.1	28.0 25.9	8.92E-04	15.6 15.4	58.7 58.1	3.00 3.01	1.07 1.06	64.8	113 1.05E+13
1250.0	26.2	8.66E-04	15.7	57.0	2.99	1.10	63.2	108	1.03E+13
275.5	26.1	8.88E-04	15.2	57.0	3.01	1.09	63.8	109	1.13E+13
301.5	26.1	8.88E-04	15.2	57.0	3.02	1.10	63.6	109	1.13E+13
305.0	25.9	8.92E-04	15.1	57.0					1.11E+13
326.5	25.9	8.92E-04	15.3	57.7	3.03	1.12	63.0	110	1.07E+13
336.5	26.1	8.88E-04	15.3	57.4					1.10E+13
350.5	26.0	8.90E-04	15.2	57.2	3.05	1.13	63.0	110	1.11E+13

Table 6.10 Bench-Scale Test Data for EC Combination

Time (hr)	Temp. (°C)	Absolute Viscosity μ (Pa*s)	Permeate Flow, Q (mL/min)	Normalized Flux, J (L/m²/hr)	Bulk DOC (mg/L)	Permeate DOC (mg/L)	DOC Rejec. (%)	Mass Loading (mg C/m²hr)	Gel Resist. (m⁻¹)
Deion. H2O	24.5	9.22E-04	15.4	60.6					R_m = 4.11E+13
0.1	22.1	9.76E-04	11.5	48.6					5.55E+12
t 0.2 0.8	22.9 22.3	9.57E-04	11.4 11.5	47.9 47.4	3.27	0.206	93.7	145	7.16E+12
3.3	24.5	9.22E-04	11.4	44.8					1.09E+13
10.8	26.9	8.72E-04	11.4	41.6	3.43	0.201	94.1	135	1.66E+13
23.6	26.3	8.84E-04	10.5	39.2	3.46	0.181	94.8	128	1.91E+13
32.8	26.5	8.88E-04	10.2	37.8					2.11E+13
4 7 45.3 70.3	26.5 25.9	8.80E-04	10.0 9.8	37.7 36.3	3.40 3.42	0.159 0.164	95.6 95.2	123 118	2.32E+13
91.8	26.0	8.90E-04	9.9	37.3	3.39	0.160	95.3	120	2.13E+13
108.3	26.8	8.74E-04	9.7	35.6					2.46E+13
115.3 139.3	26.4 26.5	8.70E-04	9.6 9.6	35.3 34.7	3.36 3.46	0.354 0.264	92.1 89.8	109 108	2.49E+13
1543	26.8	8.74E-04	9.6	35.3					2.52E+13
162.8	26.9	8.72E-04	9.7	35.5	3.45	0.281	91.9	113	2.49E+13
200.3	25.4	9.02E-04	9.3	35.6	3.36	0.322	so.4	108	2.29E+13
216.3	25.0	9.11E-04	9.3	36.0	3.44	0.328	90.5	112	2.18E+13
238.8	25.5	9.00E-04	9.3	35.5	3.31	0.236	92.9	109	2.32E+13
280.8	26.0	8.90E-04	9.5	35.7	3.37	0.210	93.8	113	2.35E+13
2843 291.3	26.216	9.00E-04	9.5 9.5	35.6 36.3	3.32	0.160	95.2	115	2.21E+13
314.3	25.9	9.05E-04	10	38.4	3.40	0.160	95.3	124	2.05E+13
323.3	26.7	8.76E-04	10	36.9					2.27E+13
332.3	26.7	8.76E-04	10	36.9	3.36	0.175	94.8	118	2.27E+13

Table 6.11 Bench-Scale Test Data for GC Combination

Time (hr)	Temp. (°C)	Absolute Viscosity μ (Pa*s)	Permeate Flow, Q (mL/min)	Normalized Flux, J (L/m²/hr)	Bulk DOC (mg/L)	Permeate DOC (mg/L)	DOC Rejec. (%)	Mass Loading (mg C/m²hr)	Gel Resist. (m^{-1})
DH_2O	24.4	9.24E-04	18.0	71.0					R_m = 2.65E+13
0.5	25.2	9.07E-04	17.6	67.8	3.40	2.11	37.9	87.5	1.77E+12
1.0	26.1	8.88E-04	17.0	63.8					4.19E+12
2.8	27.9	8.52E-04	17.2	61.2					6.82E+12
6.5	29.2	8.28E-04	16.1	55.1					1.16E+13
7.5	29.2	8.28E-04	16.0	54.8	3.45	2.18	36.8	69.6	1.18E+13
23."	29.2	8.28E-04	14.4	49.3					1.61E+13
24.6	28.5	8.41E-04	14.2	49.6	3.52	2.17	38.4	67.0	1.51E+13
26.5	27.7	8.56E-04	14.3	51.2					1.32E+13
30.0	26.9	8.72E-04	13.7	50.2					1.32E+13
31.5	26.9	8.72E-04	13.7	50.2	3.58	2.27	36.6	65.8	1.32E+13
37.5	26.9	8.72E-04	13.9	50.9					1.26E+13
47.5	27.3	8.64E-04	13.8	50.0					1.38E+13
55."	26.4	8.82E-04	13.5	50.2	3.68	2.21	39.9	76.5	1.28E+13
72.0	26.4	8.82E-04	13.3	49.5					1.33E+13
78.0	26.1	8.88E-04	13.1	49.2	3.78	2.26	40.2	74.7	1.33E+13
97.0	26.2	8.86E-04	13.1	49.0					1.35E+13
98.5	26.0	8.90E-04	13.0	46.9	3.65	2.12	41.9	74.8	1.34E+13
103.5	25.7	8.96E-04	13.0	49.4					1.28E+13
120.5	26.4	8.82E-04	13.0	48.3	3.66	2.24	36.8	68.6	1.43E+13
127.5	25.8	8.94E-04	13.0	49.2					1.30E+13
1440	26.9	8.72E-04	13.0	47.6	3.66	2.27	36.0	66.2	1.53E+13
169.0	27.3	8.64E-04	13.1	47.4	3.79	2.38	37.2	66.9	1.59E+13
193.0	27.0	8.70E-04	13.1	47.9	3.68	2.24	39.1	68.9	1.52E+13
219.0	26.3	8.84E-04	12.6	47.7	3.62	2.30	36.5	63.0	1.47E+13
240.5	26.9	8.72E-04	12.9	47.3	3.72	2.34	37.1	65.2	1.57E+13
265.5	27.3	8.64E-04	13.0	47.1	3.73	2.35	37.0	65.0	1.62E+13
314.5	27.2	8.66E-04	13.1	47.6	3.96	2.38	40.2	76.1	1.57E+13
338.0	27.9	8.52E-04	13.6	49.1	3.70	2.41	34.9	63.3	1.50E+13
363.5	27.2	8.66E-04	13.5	49.0	3.73	2.44	34.6	63.3	1.44E+13

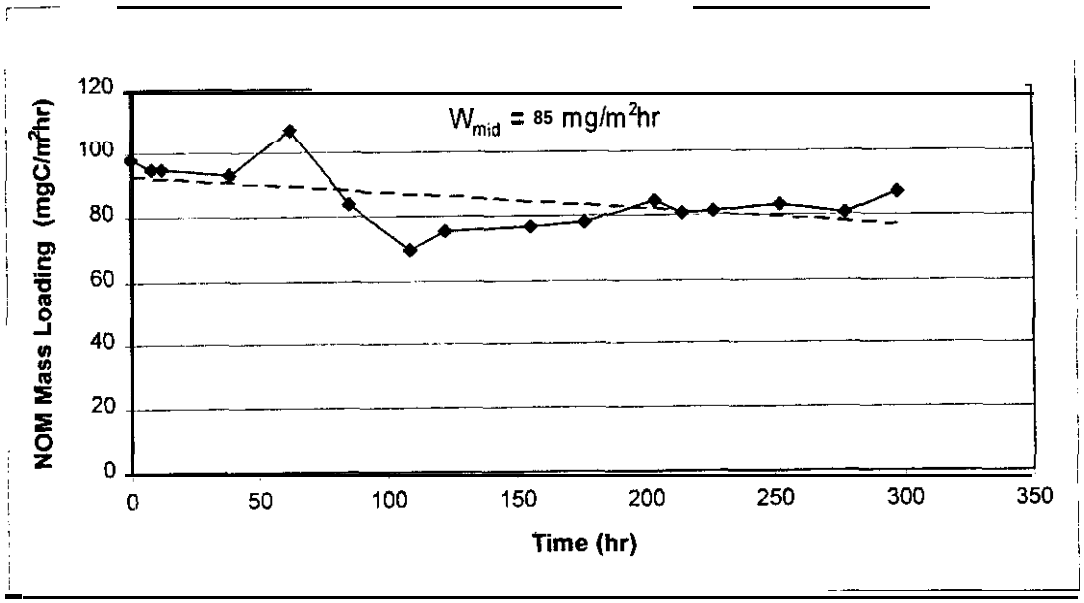

Figure 6.9 NOM Mass Loading for Bench-Scale EH Combination

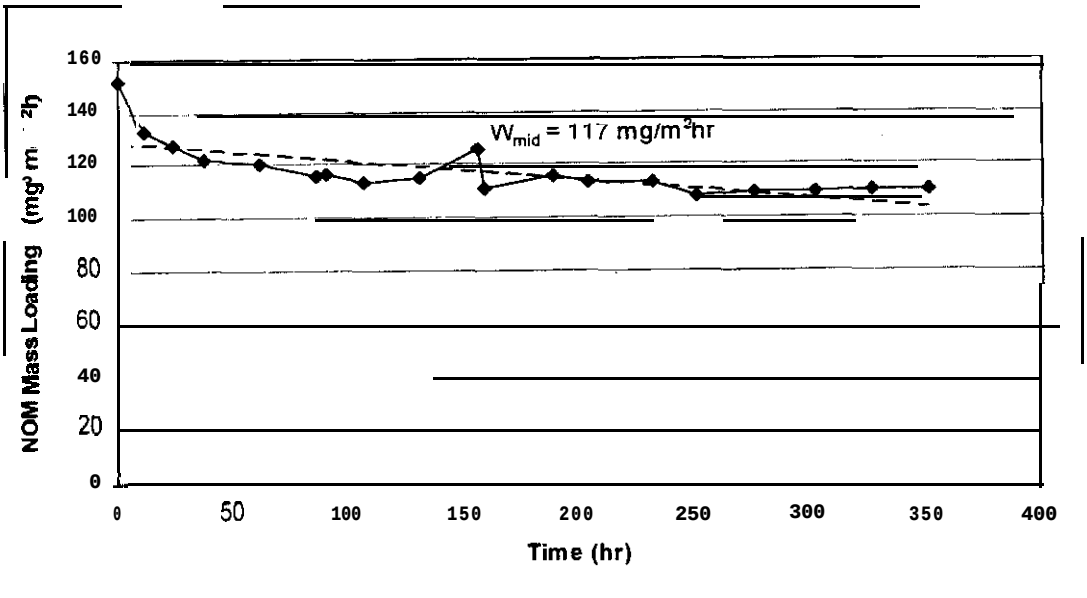

Figure 6.10 NOM Mass Loading for Bench-Scale GH Combination

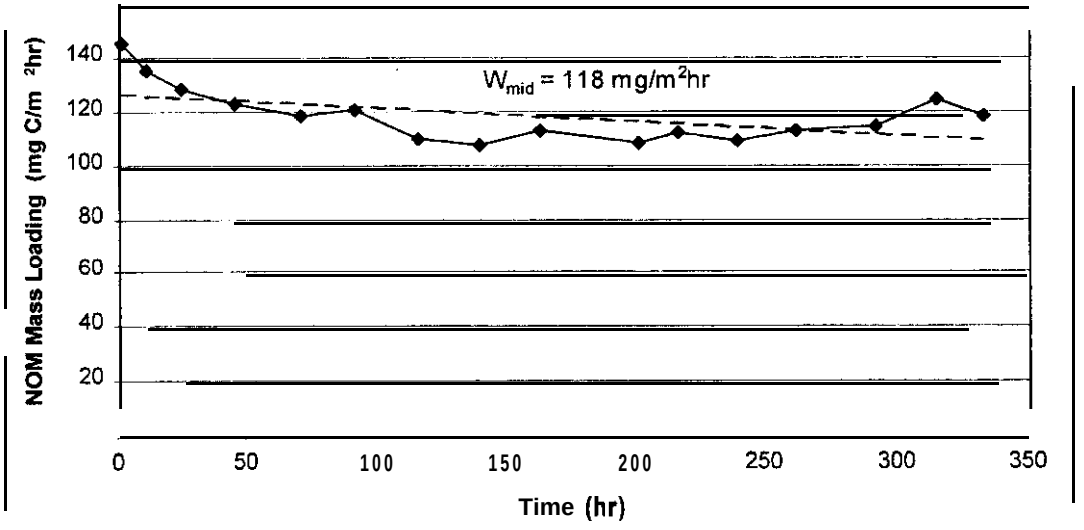

Figure 6.11 NOM Mass Loading for Bench-Scale EC Combination

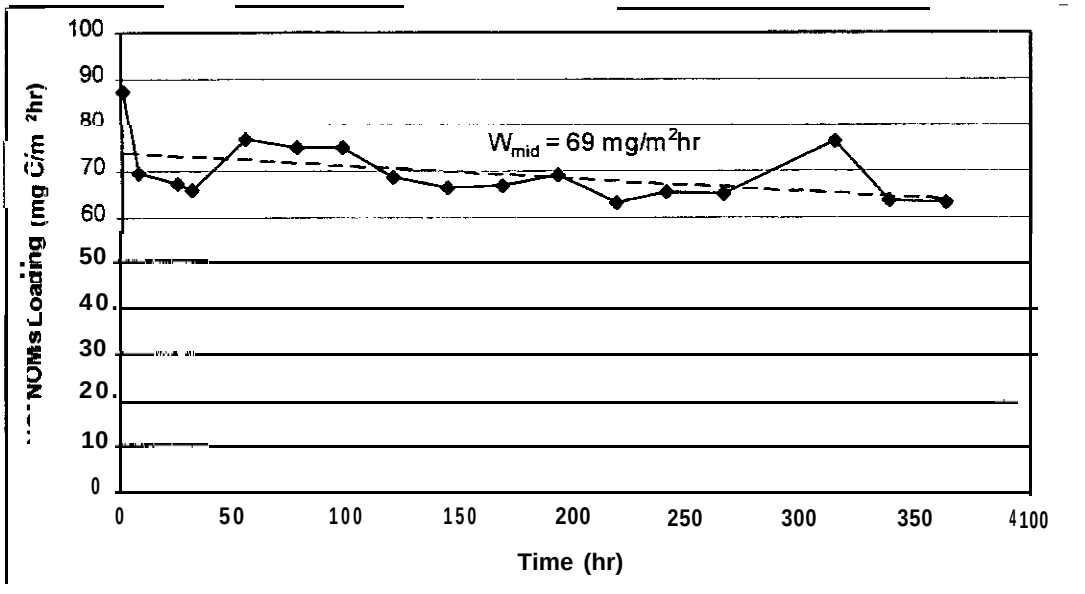

Figure 6.12 NOM Mass Loading for Bench-Scale GC Combination

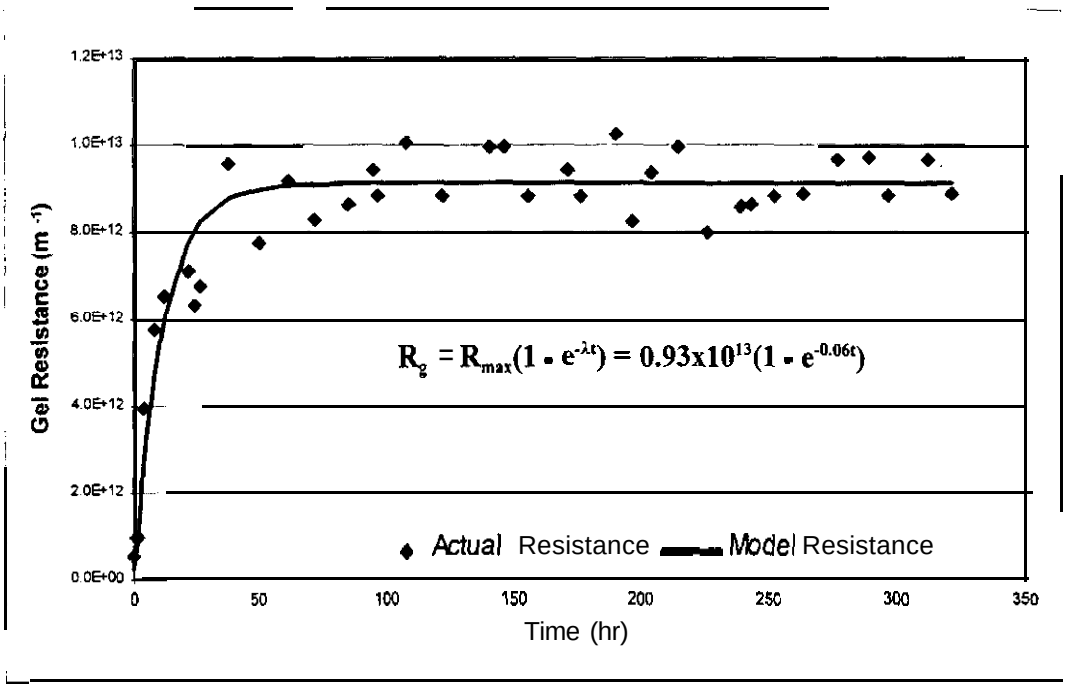

Figure 6.13 NOM Gel Resistance for Bench-Scale EH Combination

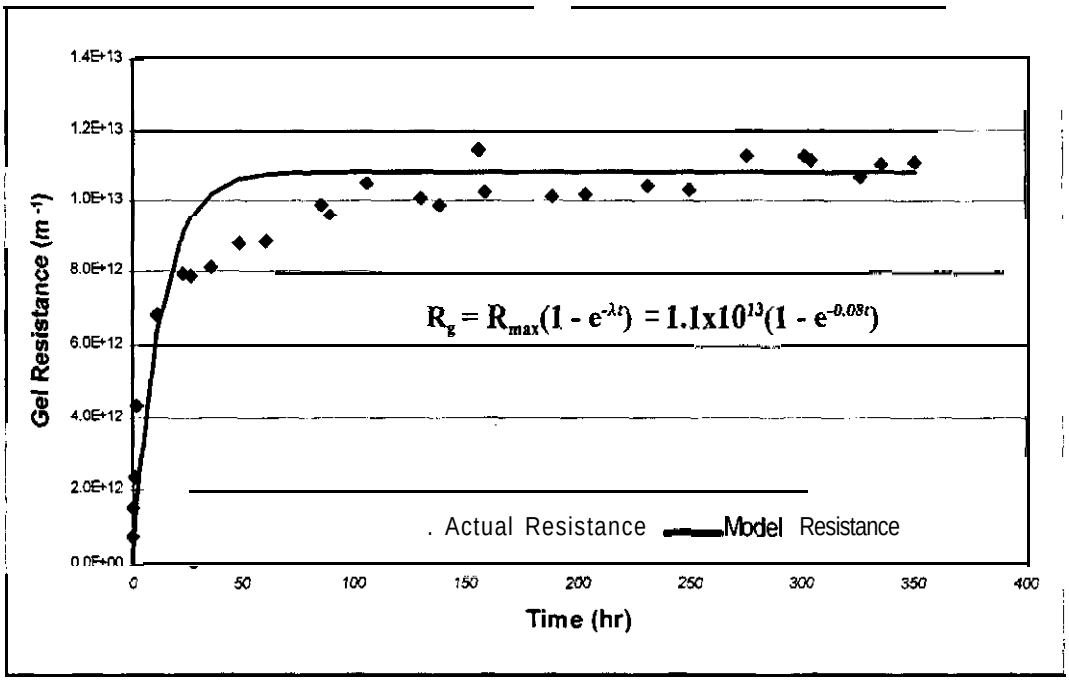

Figure 6.14 NOM Gel Resistance for Bench-Scale GH Combination

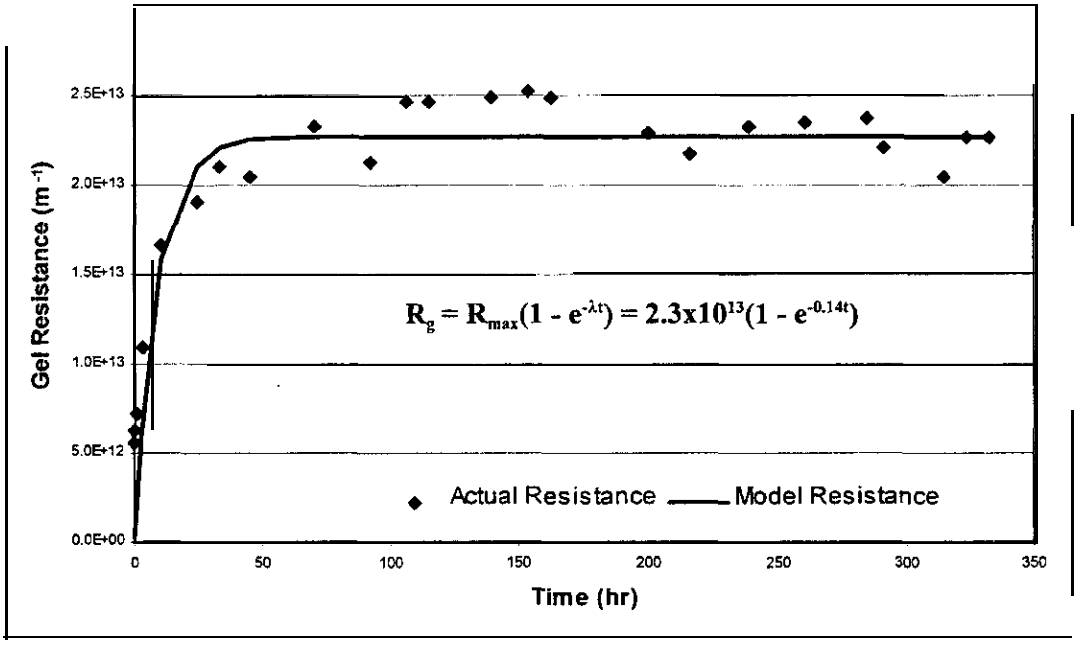

Figure 6.15 NOM Gel Resistance for Bench-Scale EC Combination

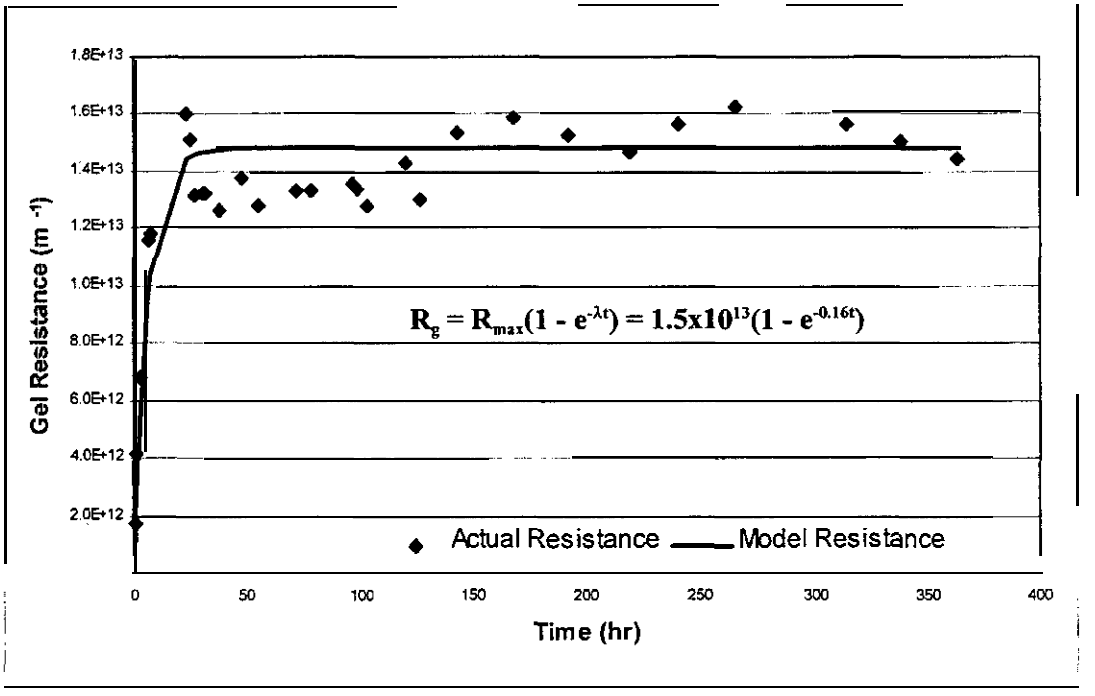

Figure 6.16 NOM Gel Resistance for Bench-Scale GC Combination

6.4.1 Propagation of Uncertainty for Bench-Scale Tests

The analysis of the propagation of uncertainty of the measured and calculated parameters for the bench-scale tests followed the same format used for the stirred cell tests. Measurements of the applied pressure and temperature in the bench-scale tests were performed in identical manner to the stirred cell tests. Differences in the equipment and operating conditions affected the calculations of permeate flux rate and osmotic pressure as described below. The uncertainties for all other calculated quantities were determined using the equations developed for the stirred ceil tests.

The membrane used in the Osmonics test cell is a rectangle that measures 19 cm x 14 cm. The uncertainty of each measurement is $\delta l = 1$ cm. The uncertainty of the calculated area is expressed using the following equation (adapted from Taylor, 1997):

$$\frac{\delta A}{A} = \sqrt{\left(\frac{\delta l}{l_1}\right)^2 + \left(\frac{\delta l}{l_2}\right)^2} \qquad (6.28)$$

The permeate flow rate, Q, was measured using a graduated cylinder and a stopwatch. The uncertainty of Q is a combination of the uncertainties in the measurement of time and volume, and is assumed to have an overall uncertainty of 10% of the measured value: $\delta Q = 0.10Q$. The uncertainty in the calculation of permeate flux rate was again determined using Eq. (6.10).

Osmotic pressure, $\Delta\pi$, in bench-scale tests occurred only when using the ESNA membrane ($\Delta\pi = 0$ for tests using the GM membrane). The osmotic pressure was negligible (An < 0.5 psi) for the EH combination, and only about 3 psi for the EC combination. Again the osmotic pressure was calculated using Eqs. (4.1) and (4.2) having an assumed uncertainty of 10%: $\delta\Delta\pi = 0.10\ An$.

The bench-scale modeling parameters (W_{mid}, R_{max}, and K) were not calculated directly but rather were determined statistically by least squares fitting. The uncertainty of W_{mid} and R_{max} due to propagation was approximated as the uncertainty of the Wand R_g values that were closest to these statistical values. The corresponding uncertainty in K was simulated using the following equation (adapted from Taylor, 1997):

$$\frac{\delta K}{K} = \sqrt{\left(\frac{\delta W_{mid}}{W_{mid}}\right)^2 + \left(\frac{\delta R_{\max}}{R_{\max}}\right)^2} \qquad (6.28)$$

6.4.2 Least Squares Uncertainty for Bench-Scale Tests

Least squares fitting was used to plot the relationships between NOM mass loading, W, vs. time and gel resistance, R_g, vs. time according to the modeling parameters developed in Eqs. (5.16 - 5.19). The fitted curves were analyzed statistically to determine the modeling parameters W_{mid}, R_{max}, and K.

The uncertainty of W_{mid} was calculated using Eq. (6.25). The parameter R_{max} was evaluated by the linearized form of Eq. (5.19). The uncertainty of R_{max} was calculated using Eq. (6.25) for R_g and the following equation (Taylor, 1997):

$$\sigma_A = \sigma_y \sqrt{\frac{\sum x^2}{N\sum x^2 - \left(\sum x^2\right)}} \tag{6.29}$$

The NOM accumulation coefficient, *K,* **was** calculated as the ratio R_{max}/W_{mid} and, therefore, the uncertainty in K was determined by the standard propagation formula (Taylor, 1997):

$$\sigma_K = K\sqrt{\left(\frac{\sigma_A}{A}\right)^2 + \left(\frac{\sigma_{W_{mid}}}{W_{mid}}\right)^2} \tag{6.30}$$

6.4.3 Discussion of Bench-Scale Results

The plots of the NOM mass loading function, W(t), show a gradual decrease with time. The dashed lines are a least squares fit using linear regression. The plots illustrate that the step input used to describe W(t) for the gel resistance model (Eqs. [5.16 - 5.171) is a valid approximation. The midpoint of each regression line, W_{mid}, was taken as the approximate value of the step input.

The plots of NOM gel resistance, R_g, increase exponentially with time and approach a maximum steady value, R_{max}, for all four source water-membrane combinations. These maximum gel resistance values divided by their respective step inputs, W_{mid}, yields the Kvalues for the bench-scale resistance model, Eq. (5.19). The modeling parameters are summarized in Table 6.12. The following observations are made with respect to the NOM mass loading values, W_{mid}, from Table 6.12:

- $W_{GH} > W_{EH}$ due to the greater permeate flux rate of the GM ultrafiltration membrane.
- $W_{GC} < W_{EC}$ due to the much lower NOM rejection of the GM ultrafiltration membrane. The GM membrane was much less efficient in rejecting the CR NOM as compared to HT NOM resulting in a much greater concentration of NOM at the membrane surface.
- $W_{EC} > W_{EH}$ because the NOM concentration of the CR feedwater was greater than the HT water while NOM rejection was about the same.

The NOM accumulation coefficient, K, represents the proportion of the NOM mass loading, W_{mid}, that is incorporated into the gel layer. The K parameter is comprised of constants that describe properties of the feedwater, NOM, and membrane which influence NOM-membrane interactions. As shown in Table 6.12, the K values for the tests using CR

Table 6.12 Bench-Scale Modeling Parameters

Test	W_{mid} (mg/m²hr)	Uncertainty,% Propag. Analysis	Uncertainty,% Least Sq. Analysis'	R_{max} (m^{-1})	Uncertainty, % Propag. Analysis	Uncertainty, % Least Sq. Analysis'	K (mhr/mg)	Uncertainty, % Propag. Analysis	Uncertainty, % Least Sq. Analysts'
EH	**85**	11	20	0.93E13	42	25	1.1E11	43	32
GH	120	12	13	1.1E13	33	24	0.92E11	35	27
EC	120	11	14	2.3E13	30	38	1.9E11	32	40
GC	69	18	17	1.5E13	30	29	2.2E11	35	33

'Percent uncertainty for least squares analysis based on two standard deviations (95% confidence level): % uncertainty = $2\sigma_y/y$.

water are about double the corresponding values for the tests using HP water. The larger Kvalues for CR water are attributed to the much greater ionic strength of the CR water. The greater ionic strength reduces the electrostatic repulsion between the NOM and membrane which leads to increased gel resistance.

The exponential increase and subsequent maximum steady value of gel resistance with time was predicted by the gel resistance model. Additionally, test data support the theory and definition of the NOM accumulation coefficient, *K,* in terms of the properties of the feedwater, NOM, and membrane.

6.5 Pilot-Scale Results

A pilot-scale test was conducted for each of the four source water-membrane combinations using the methods and apparatus described in Section 4.3.3. The raw data and calculated parameters are presented in Tables 6.13 - 6.16. Plots of the NOM mass loading function, W(t), and NOM gel resistance, R_g, are shown on Figures 6.17 - 6.24.

Table 6.13 Pilot-Scale Test Data for EH Combination

Time (hr)	Temp. (°C)	Absolute Viscosity μ (Pa·s)	Permeate Flow, Q (L/min)	Normalized Flux, J (L/m²/hr)	Bulk DOC (mg/L)	Permeate DOC (mg/L)	DOC Rejec. (%)	Mass Loading (mg C/m²hr)	Gel Resist. (m^{-1})
Deion. H_2O	22.7	9.62E-04	1.25	30.9					R_m = 7.47E+13
1	23.8	9.37E-04	1.20	28.7	3.24	0.21	93.5	66.9	1.94E+12
7	24.4	9.24E-04	1.20	28.2					4.03E+12
12	24.4	9.24E-04	1.20	28.2					4.03E+12
24	24.4	9.24E-04	1.16	27.7	3.24	0.16	94.4	64.8	5.16E+12
39	24.6	9.19E-04	1.17	27.3					6.47E+12
51	24.3	9.26E-04	1.17	27.6	3.24	0.16	95.1	84.9	5.38E+12
63	24.4	9.24E-04	1.17	27.5					5.74E+12
72	24.4	9.24E-04	1.16	27.2	3.24	0.18	944	83.4	6.33E+12
a4	24.3	9.26E-04	1.13	26.6					7.79E+12
96	24.3	9.26E-04	1.12	26.4	3.24	0.20	93.8	80.2	8.42E+12
108	24.3	9.26E-04	1.11	26.2					9.06E+12
120	24.3	9.26E-04	1.10	25.9	3.38	0.22	93.5	81.9	9.71E+12
132	24.3	9.26E-04	1.10	25.9					9.71E+12
14%	24.3	9.26E-04	1.08	25.4	3.38	0.2%	92.3	79.4	1.11E+13
160	24.3	9.26E-04	1.09	25.7					1.04E+13
172	24.3	9.26E-04	1.07	25.2	3.38	0.21	93.8	79.9	1.17E+13
184	24.2	9.28E-04	1.06	25.0					1.20E+13
196	24.4	9.24E-04	1.07	25.1	3.38	0.19	94.4	80.2	1.21E+13
20%	24.3	9.26E-04	1.06	25.0					1.24E+13
220	24.2	9.28E-04	1.06	25.0					1.20E+13
292	24.4	9.24E-04	1.04	24.5 24.7 24.4	3.41 3.41	0.25 0.28	91.8	78.4 76.5	1.43E+13
316	24.3	9.26E-04	1.02	24.0					1.54E+13
340	24.3	9.26E-04	1.02	24.0	3.22	0.24	92.5	71.6	1.54E+13
364	24.3	9.26E-04	1.01	23.8					1.62E+13
388	24.2	9.28E-04	1.00	23.6	3.22	0.20	93.6	71.4	1.65E+13
412	24.2	9.28E-04	1.01	23.9					1.57E+13
436	24.2	9.28E-04	0.99	23.4	3.07	0.21	93.2	66.9	1.73E+13
460 484	24.2 24.3	9.26E-04	0.99 0.98	23.4 23.1	3.07	0.18	94.1	66.7	1.86E+13

Table 6.14 Pilot-Scale Test Data for GH Combination

Time (hr)	Temp. (°C)	Absolute Viscosity μ (Pa*s)	Permeate Flow, Q (L/min)	Normalized Flux, J ($L/m^2/hr$)	Bulk DOC (mg/L)	Permeate DOC (mg/L)	DOC Rejec. (%)	Mass Loading (mgC/m^2hr)	Gel Resist. (m^{-1})
Deion. H_2O	22.7	9.62E-04	2.11	54.2					R_m = 2.38E+13
1	23.0	9.55E-04	1.90	48.4	3.28	1.20	63.4	100.6	4.13E+12
7	24.6	9.19E-04	2.02	49.1					4.81E+12
12	24.4	9.24E-04	1.99	48.6					4.93E+12
24	24.3	9.26E-04	1.97	48.3	3.28	1.22	62.8	99.4	5.07E+12
39	24.3	9.26E-04	1.91	46.6					5.98E+12
51	24.4	9.24E-04	1.88	45.9	3.28	1.21	63.1	95.1	6.61E+12
63	24.5	9.22E-04	1.84	44.8					7.44E+12
72	24.5	9.22E-04	1.81	44.1	3.28	1.19	63.7	92.1	7.96E+12
84	24.2	9.28E-04	1.77	43.5					8.16E+12
96	24.3	9.26E-04	1.73	42.4	3.28	1.31	60.1	83.5	9.08E+12
108	24.2	9.28E-04	1.69	41.6					9.68E+12
120	24.2	9.28E-04	1.67	41.0	3.47	1.38	60.2	85.8	1.01E+13
132	24.2	9.28E-04	1.64	40.3					1.07E+13
148	24.2	9.28E-04	1.64	40.3	3.47	1.48	67.3	80.2	1.07E+13
160	24.2	9.28E-04	1.63	40.1					1.09E+13
172	24.1	9.30E-04	1.67	38.7	3.47	1.42	59.1	79.3	1.20E+13
184	24.2	9.28E-04	1.59	39.1					1.18E+13
196	24.3	9.26E-04	1.68	38.7	3.47	1.40	59.7	80.1	1.22E+13
208	24.3	9.26E-04	1.55	38.0					1.29E+13
220	24.5	9.22E-04	1.53	37.3					1.38E+13
244	26.2	9.07E-04	1.53	36.5	3.18	1.26	60.4	70.1	1.52E+13
268	25.1	9.09E-04	1.54	36.9					1.47E+13
292	25.2	9.07E-04	1.62	36.3	3.18	1.31	58.8	67.8	1.54E+13
316	25.2	9.07E-04	1.51	36.0					1.57E+13
340	24.6	9.22E-04	1.5	36.5	3.42	1.29	62.3	77.8	1.45E+13
364	24.7	9.17E-04	1.49	36.1					1.52E+13
388	24.5	9.22E-04	1.60	36.5	3.42	1.28	63.2	78.9	1.45E+13
412	24.4	9.24E-04	1.46	35.7					1.54E+13
436	24.4	9.24E-04	1.44	35.2	3.62	1.36	61.4	76.0	1.59E+13
460	24.4	9.24E-04	1.46	35.7					1.54E+13
484	24.4	9.24E-04	1.47	35.9	3.52	1.31	62.8	79.4	1.51E+13

Table 6.16 Pilot-Scale Test Data for EC Combination

Time (hr)	Temp. (°C)	Absolute Viscosity μ (Pa*s)	Permeate Flow, Q (L/min)	Normalized Flux, J (L/m²/hr)	Bulk DOC (mg/L)	Permeate DOC (mg/L)	DOC Rejec. (%)	Mass Loading (mgC/m²hr)	Gel Resist. (m^{-1})
Deion. H_2O	32	7.79E-04	0.93	17.5					R_m = 7.52E+13
2	29.7	8.19E-04	0.85	17.1	3.53	0.32	90.9	54.8	9.78E+12
15	28.8	8.36E-04	0.87	17.9					1.18E+13
18	33.4	7.57E-04	0.94	16.9					2.32E+13
30	30.2	8.10E-04	0.73	14.4	4.33	0.28	93.5	58.5	2.67E+13
42	37.2	7.00E-04	0.92	14.8					2.29E+13
50	33.3	7.58E-04	0.81	14.6	3.24	0.22	93.2	44.2	2.12E+13
60	35.8	7.20E-04	0.83	13.9					3.04E+13
70	38.5	7.10E-04	0.87	14.3	3.06	0.35	88.6	38.7	3.02E+13
84	36.9	7.04E-04	0.87	14.1					3.14E+13
90	32.8	7.66E-04	0.83	15.2	3.22	0.40	87.6	42.9	2.07E+13
100	31.9	7.81E-04	0.80	15.1					2.36E+13
110	28.5	8.41E-04	0.67	13.9	2.86	0.33	88.5	35.3	2.86E+13
120	33.5	7.55E-04	0.72	12.9					3.06E+13
140	33.6	7.53E-04	0.75	13.4	2.92	0.28	90.4	35.4	2.77E+13
185	29.2	8.28E-04	0.64	13.0					2.77E+13
215	30.3	8.08E-04	0.69	13.6	2.71	0.25	90.8	33.5	3.26E+13
235	33.7	7.52E-04	0.78	13.6					3.73E+13
250	27.2	8.66E-04	0.59	12.8	3.23	0.26	92.0	37.9	3.30E+13
260	31.7	7.84E-04	0.75	14.2	3.54	0.35	90.1	45.3	3.74E+13
272	29.2	8.28E-04	0.68	13.9	3.53	0.21	94.1	48.0	3.95E+13
292	26.5	8.80E-04	0.62	13.7	3.16	0.37	88.3	36.2	3.47E+13
320	29.9	8.16E-04	0.71	14.2	2.43	0.26	89.3	30.8	3.89E+13
332	26.9	8.72E-04	0.67	14.6					3.37E+13
342	29.5	8.23E-04	0.71	14.3	2.94	0.30	89.8	37.9	3.66E+13
362	30.1	8.12E-04	0.72	14.3	2.75	0.18	93.5	36.7	3.83E+13
382	29.5	8.23E-04	0.69	13.9	2.57	0.22	91.4	32.8	3.84E+13
410	30.5	8.05E-04	0.74	14.5	2.67	0.26	90.3	35.0	3.89E+13
424	27.8	8.54E-04	0.68	14.4	2.72	0.15	94.5	37.1	3.52E+13
475	27.2	8.66E-04	0.67	14.5					3.64E+13
492	27.7	8.56E-04	0.66	14.1	2.51	0.26	89.6	31.6	3.89E+13

Table 6.16 Pilot-Scale Test Data for GC Combination

Time (hr)	Temp. (°C)	Absolute Viscosity μ (Pa's)	Permeate Flow, Q (L/min)	Normalized Flux, J (L/m²/hr)	Bulk DOC (mg/L)	Permeate DOC (mg/L)	DOC Rejec. (%)	Mass Loading (mgC/m²hr)	Gel Resist. (m^{-1})
Initial H_2O	32	7.79E-04	2.11	39.6					R_m = 2.40E+13
2	25.8	8.94E-04	1.89	42.6	2.56	1.01	60.5	66.0	7.57E+12
15	21.7	9.85E-04	1.60	40.7					6.35E+12
25	25.9	8.92E-04	1.67	37.5					1.23E+13
40	22.3	9.71E-04	1.60	40.0	2.64	1.12	57.6	60.8	6.69E+12
52	24.5	9.22E-04	1.67	39.1					8.06E+12
62	27.2	8.66E-04	1.80	38.9	2.62	1.00	61.8	63.1	1.04E+13
78	24.5	9.22E-04	1.50	35.1	2.45	1.14	53.5	46.0	9.14E+12
a	22.1	9.76E-04	1.48	37.2					8.53E+12
98	22.3	9.71E-04	1.44	36.0	2.51	1.06	57.8	52.2	9.48E+12
110	22.5	9.66E-04	1.38	34.3	2.69	1.21	56.0	50.7	1.45E+13
122	21.1	9.99E-04	1.20	31.1					1.38E+13
134	23.6	9.41E-04	1.31	31.5	2.51	1.14	54.6	43.2	2.01E+13
146	20.1	1.02E-03	1.22	32.5					1.27E+13
158	22.6	9.59E-04	1.32	32.5	2.54	1.18	53.5	44.2	1.72E+13
170	23.4	9.46E-04	1.29	31.2	2.62	1.21	53.8	44.0	1.76E+13
182	22.3	9.71E-04	1.27	31.7					1.56E+13
194	25.2	9.07E-04	1.33	30.5	2.49	1.11	55.4	42.1	2.01E+13
215	25.3	9.05E-04	1.36	31.1					2.04E+13
245	22.7	9.62E-04	1.27	31.4	2.59	1.06	59.1	48.0	1.69E+13
258	23.3	9.48E-04	1.34	32.5	2.66	1.15	65.4	46.5	1.73E+13
276	22.0	9.78E-04	1.29	32.5	2.66	1.12	58.2	50.7	1.72E+13
303	22.1	9.76E-04	1.20	30.2					1.91E+13
335	16.5	1.12E-03	0.87	25.6	2.71	1.01	62.7	43.9	1.75E+13
356	17.1	1.10E-03	0.89	25.9	2.56	0.99	61.3	40.7	1.73E+13
391	20.6	1.01E-03	1.03	26.9	2.50	1.13	54.8	36.9	2.20E+13
418	19.6	1.04E-03	1.01	27.3	2.48	1.17	52.8	35.8	2.07E+13
448	18.3	1.07E-03	0.95	26.7	2.51	1.21	51.8	34.7	1.93E+13
482	17.6	1.09E-03	0.91	26.1	2.81	1.15	59.1	43.4	2.11E+13

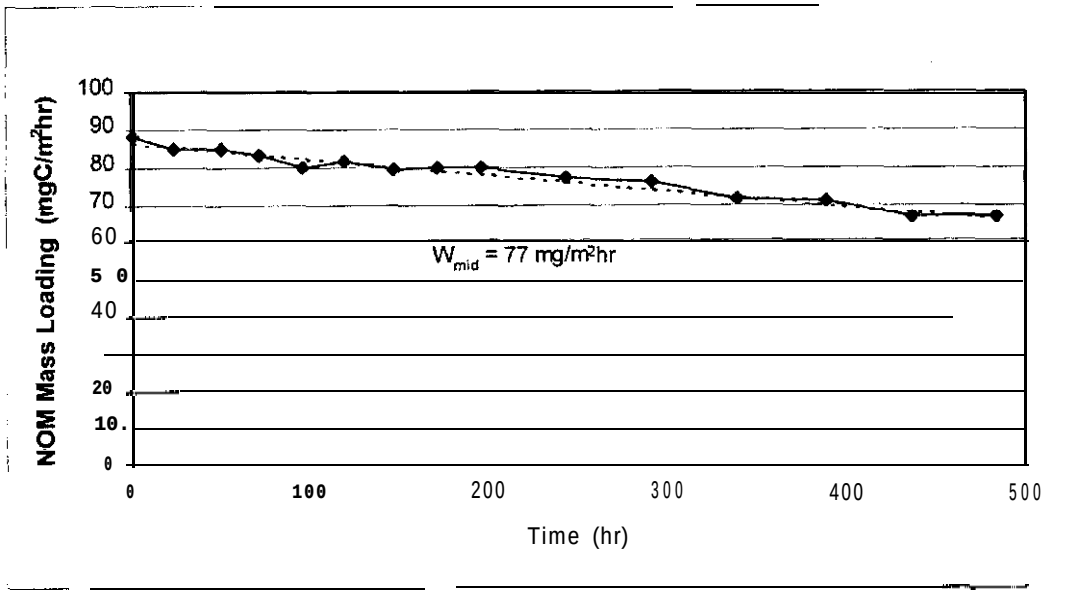

Figure 6.17 NOM Mass Loading for Pilot-Scale EH Combination

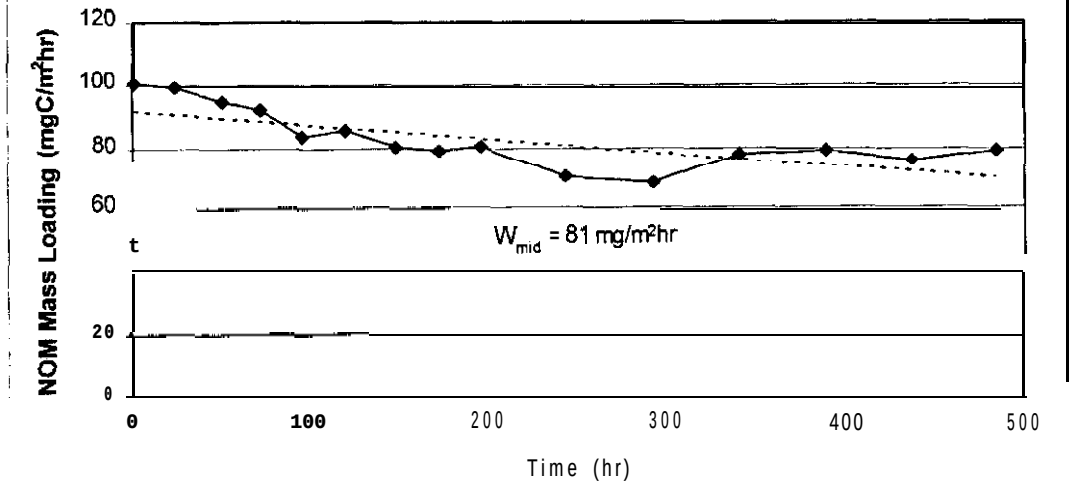

Figure 6.18 NOM Mass Loading for Pilot-Scale GH Combination

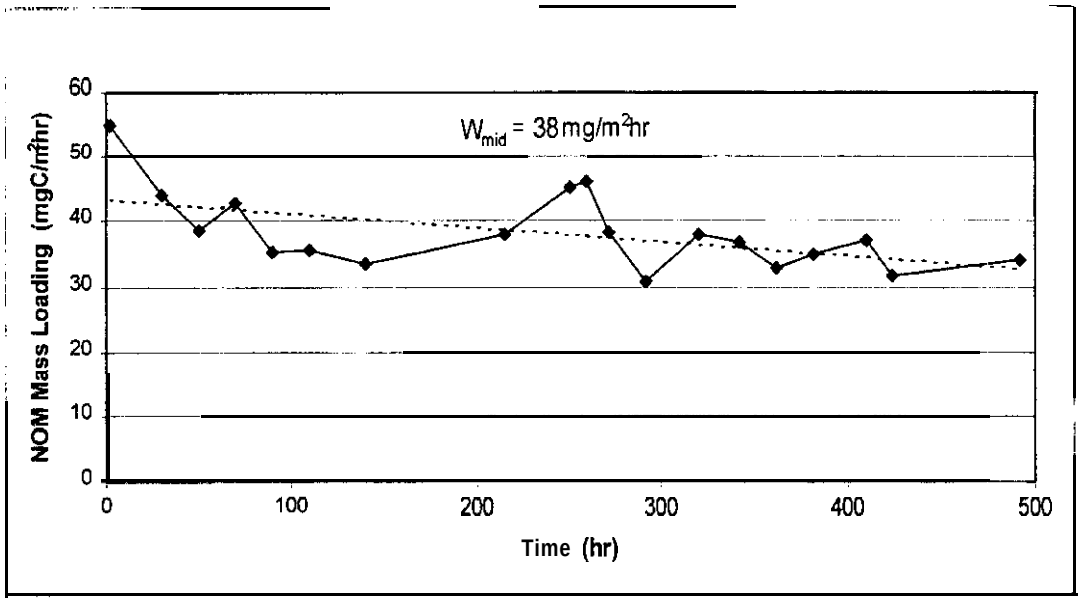

Figure 6.19 NOM Mass Loading for Pilot-Scale EC Combination

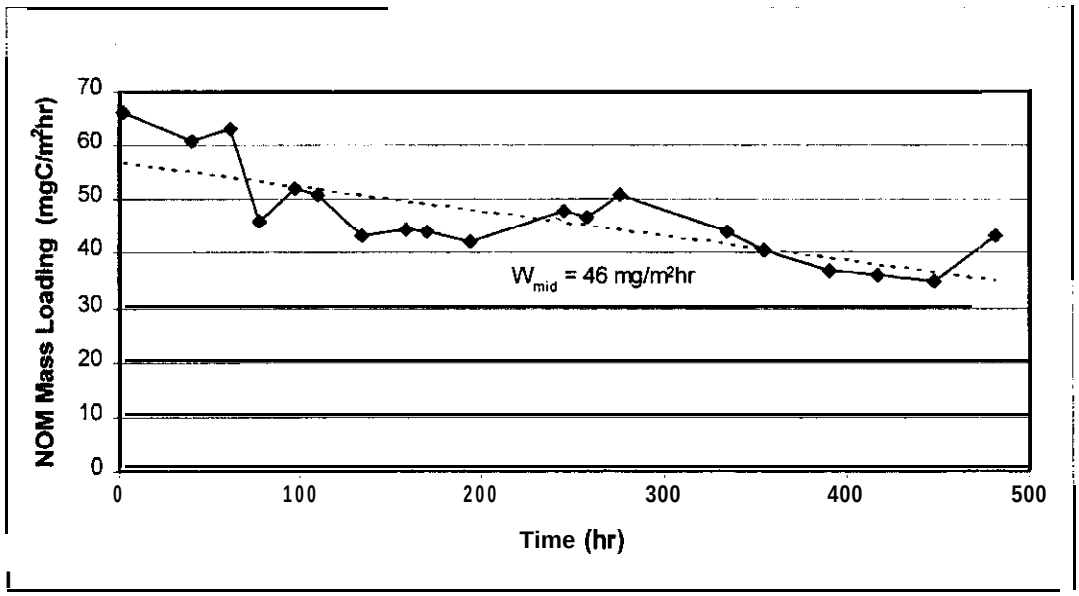

Figure 6.20 NOM Mass Loading for Pilot-Scale GC Combination

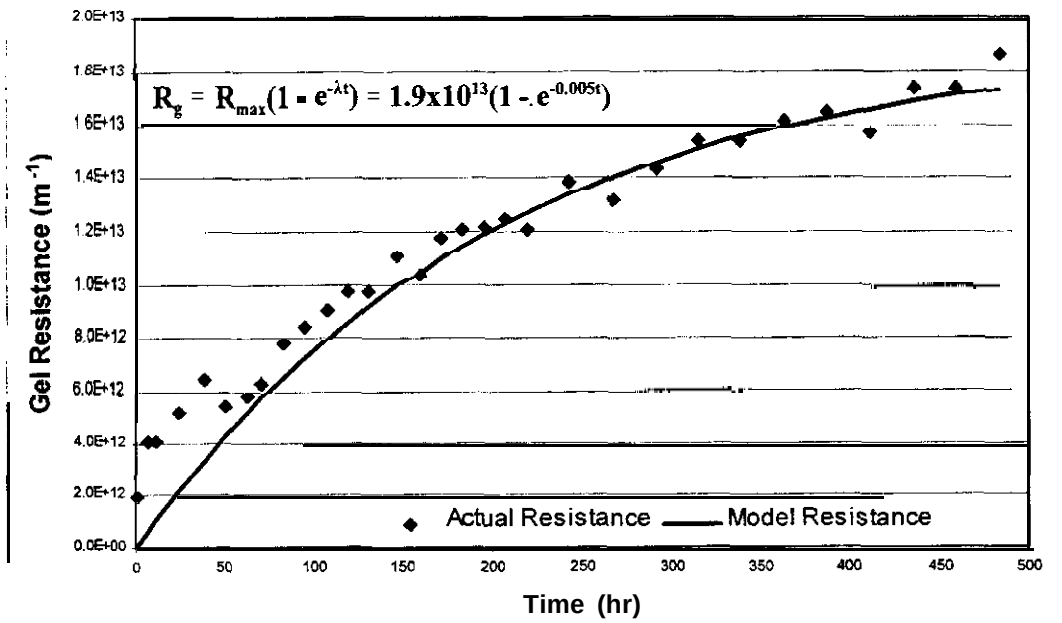

Figure 6.21 NOM Gel Resistance for Pilot-Scale EH Combination

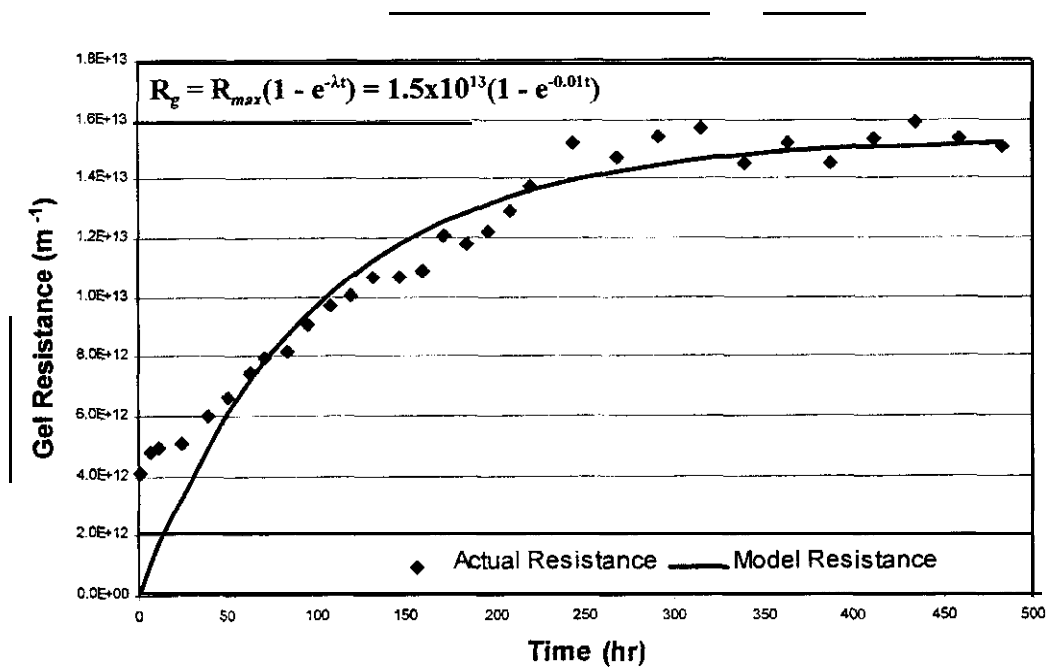

Figure 6.22 NOM Gel Resistance for Pilot-Scale GH Combination

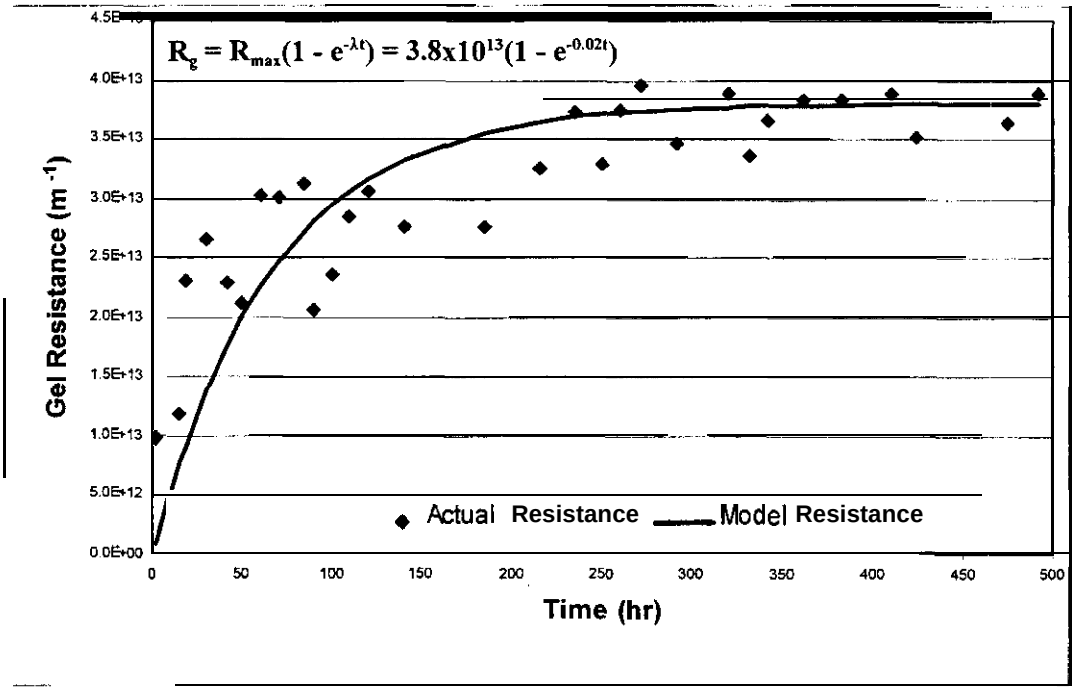

Figure 6.23 NOM Gel Resistance for Pilot-Scale EC Combination

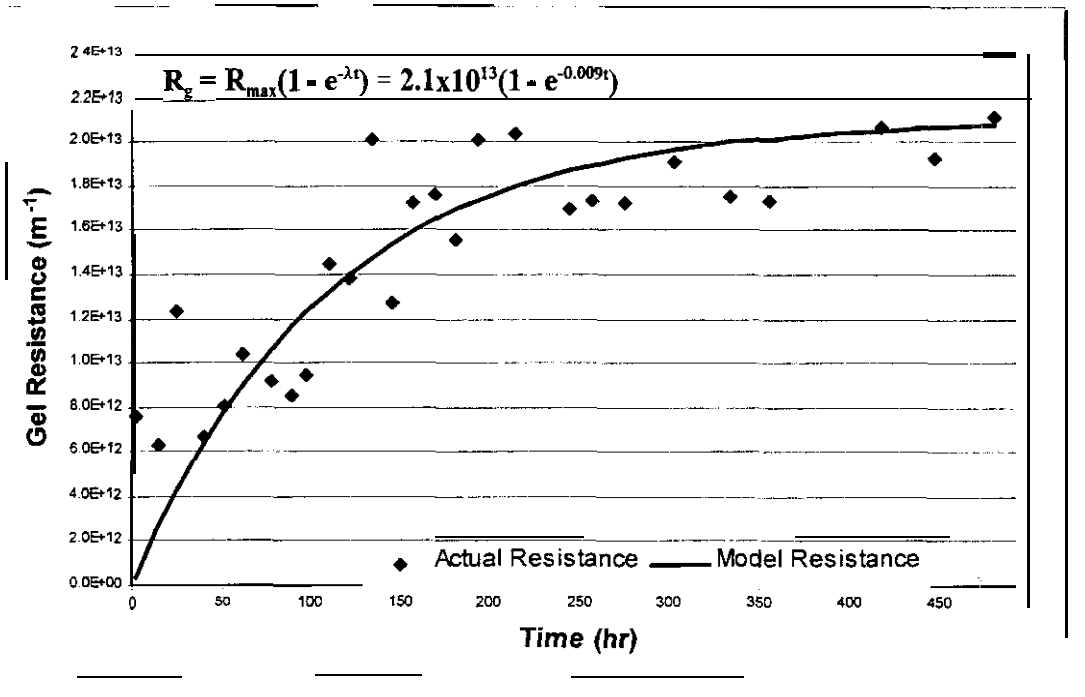

Figure 6.24 NOM Gel Resistance for Pilot-Scale GC Combination

6.5.1 Propagation of Uncertainty for Pilot-Scale Tests

The pilot-scale test apparatus (Figure 4.3) employed superior electronic instrumentation for data collection as compared to the analog and manual measurements for the stirred cell and bench-scale tests. Measurements of flow rate, temperature, and pressure were performed using a combination of electronic sensors and indicators. The combined uncertainty of each measurement is the sum of the individual uncertainties for each instrument component used in the measurement. A review of manufacturer's literature for pilot instrumentation provided the basis for the following estimates of measurement uncertainty. The resulting assumed instrumentation uncertainties are:

- Permeate flow rate, 3% random, 0.1 L/min systematic
- Temperature, 2% random, 1°C systematic
- Pressure, 1% random, 2 psi systematic

Pressure measurements were taken at the inlet (feedwater) and outlet (concentrate) of each 2.5 x 40 in. membrane element. Permeate flow exited the system to atmospheric pressure; however, it is assumed that a small, permeate pressure provided the driving force for the permeate to flow through the permeate carrier and system plumbing. This permeate pressure was not measured but was assumed to be about 5 psi. The average applied pressure

for the pilot tests was estimated using the following equation:

$$\Delta P_{avg} \approx \frac{P_f + P_c}{2} - 5 \tag{6.31}$$

where: ΔP_{avg} = average applied pressure across element, psi

P_f = measured feed pressure, psi

P_c = measured concentrate pressure, psi

The pressure distribution along the membrane element was not investigated and is unknown. The pressure difference between the inlet and outlet ($P_f - P_c$) did not exceed 7 psi. Therefore, the actual average applied pressure does not differ significantly from that calculated by Eq. (6.31) which assumes a linear pressure distribution. It does, however, add uncertainty to the pressure calculations. The uncertainty of Eq. (6.31) due to the unknown pressure distribution is assumed to be 2 psi. The overall uncertainty in the applied pressure calculation is calculated using the following equations (adapted from Taylor, 1997):

$$\delta P_f = \sqrt{\left(0.01 P_f\right)^2 + 2^2} \tag{6.32}$$

$$\delta P_c = \sqrt{\left(0.01 P_c\right)^2 + 2^2} \tag{6.33}$$

$$\delta \Delta P_{avg} = \sqrt{\left(\frac{1}{2}\delta P_f\right)^2 + \left(\frac{1}{2}\delta P_c\right)^2 + 2^2} \tag{6.34}$$

The quantity of membrane area used to calculate the permeate flux rate was taken as the nominal membrane area provided by the manufacturer. The uncertainty of this quantity is assumed to be 6% of nominal membrane area: $\delta A = 0.06A$. The analysis of the propagation of uncertainty of the measured and calculated parameters for the pilot-scale tests followed the same format and equations developed for the bench-scale test analysis.

6.5.2 Least Squares Uncertainty for Pilot-Scale Tests

Least squares fitting was employed to correlate the NOM mass loading, W, and the gel resistance, R_g, with the modeling parameters: W_{mid}, R_{max}, and K. The uncertainty analysis based on the least squares fitting followed the same procedures and equations developed for the bench-scale test analysis.

6.5.3 Discussion of Pilot-Scale Results

The plots of the NOM mass loading function, W(t), show a gradual decrease with time. The dashed lines are a least squares fit using linear regression. The plots illustrate that the step input used to describe W(t) for the gel resistance model (Eqs. [5.16 - 5.17]) is a valid approximation. The midpoint of each regression line, W_{mid}, was taken as the approximate value of the step input.

The plots of NOM gel resistance, R_g, increase exponentially with time and approach a maximum steady value, R_{max}, for all four source water-membrane combinations. These maximum gel resistance values divided by their respective step inputs, W_{mid}, yields the *K* values for the pilot-scale resistance model, Eq. (5.19). The modeling parameters are summarized in Table 6.17. The following observations are made with respect to the NOM mass loading values, W_{mid}, from Table 6.17:

- $W_{GH} \approx W_{EH}$ because the difference in permeate flux rate is offset by the difference in NOM rejection.
- $W_{GC} \approx \frac{1}{2} W_{EC}$ and $W_{EC} \approx \frac{1}{2} W_{EH}$ due to the lower flux rate achieved in the pilot tests using CR water. The pilot system using CR water was operated at about 20% below the target pressures (due to operator and equipment error) for both the ESNA and GM membranes.

The NOM accumulation coefficient, *K*, represents the proportion of the NOM mass loading, W_{mid}, that is incorporated into the gel layer. The *K* parameter is comprised of constants that describe properties of the feedwater, NOM, and membrane which influence NOM-membrane interactions. As shown in Table 6.17, the K values for the tests using CR water are 2 - 4 times greater than the corresponding values for tests using HT water. The larger *K* values for CR water are attributed to the much greater

Table 6.17 Pilot-Scale Modeling Parameters

Test	W_{mld} (mg/m²hr)	Uncertainty,% Propag. Analysis	Uncertainty,% Least Sq. Analysis'	R_{max} (m^{-1})	Uncertainty, % Propag. Analysis	Uncertainty, % Least Sq. Analysis'	K (mhr/mg)	Uncertainty, % Propag. Analysis	Uncertainty, % Least Sq. Analysis'
EH	77	10	3.5	1.9E13	48	8.6	2.5E11	49	9.2
GH	81	12	25	1.5E13	22	7.7	1.9E11	25	19
EC	38	72	27	3.8E13	31	17	10E11	34	32
GC	46	13	25	2.1E13	20	9.0	4.5E11	24	26

'Percent uncertainty for least squares analysis based on two standard deviations (95% confidence level): % uncertainty = $2\sigma_y/y$.

ionic strength of the CR water. The greater ionic strength reduces the electrostatic repulsion between the NOM and membrane which leads to increased gel resistance.

The exponential increase and subsequent maximum steady value of gel resistance with time was predicted by the gel resistance model. Additionally, test data support the theory and definition of the NOM accumulation coefficient, ***K,*** in terms of the properties of the feedwater, NOM, and membrane.

6.6 Comparison of Scales of Operation

A principal objective of this research was to compare NOM fouling of membranes at different scales of operation. Results from membrane tests are frequently used to predict performance at larger scales of operation. Proper interpretation of test results, however, requires an understanding of the mechanical similarity between the scales of operation, Mechanical! similarity consists of both geometric and dynamic similarity (Lindeburg, 1992).

6.6.1 Comparison of Geometric Similarity

Geometric similarity refers to scale in length, area, and volume. For membrane testing, the primary geometric parameters that affect similitude of scale are the volume of water per unit of time (feedwater flow rate) and the

active area of membrane surface. For the tests conducted, these parameters increased almost in proportion to each other by the orders of magnitude shown in Table 6.18.

Table 6.18 Scale Comparison of Flow Rate and Membrane Area

Scale of Operation	Feedwater Flow Rate (L/min)	Membrane Surface Area (m^2)
Laboratory stirred cell	2.0×10^{-3}	3.0×10^{-3}
Bench scale	7.0×10^{-1}	1.5×10^{-2}
Pilot scale	1.1×10^{0}	2.6×10^{0}

6.6.2 Comparison of Dynamic Similarity

Dynamic similarity refers to the scale of forces that affect membrane operation. These forces result from pressure, viscosity, inertia (feedwater velocity), concentration gradient, etc. The intent of the experimental methods was to minimize the differences in these dynamic forces between the scales of testing in order to study the influence of NOM-membrane interactions on NOM fouling. Significant differences in dynamic forces were introduced, however, due to the operational constraints described below:

1) Viscous forces varied considerably between the individual tests and between the scales of operation due to changes in ambient temperature. Calculations of absolute viscosity and permeate flux rate

included empirical correlations with temperature to compensate for the changes viscous forces. Dynamic similarity between scales of operation was not significantly compromised with regard to viscosity.

2) Laboratory stirred cell tests are conducted in a dead-end filtration mode which allows the rejected solute to remain in the feedwater reservoir. Consequently, the NOM concentration of the bulk feedwater steadily increases through time.

In contrast, bench- and pilot-scale tests are operated in a crossflow filtration mode which carries the rejected solute away from the membrane surface in a waste stream that exits the system. Under these conditions, the NOM concentration of the bulk feedwater remains at a steady level through time. The lower, steady NOM concentration in the bulk feedwater of the bench- and pilot-scale tests should produce lower rates of NOM fouling and flux decline as compared to the laboratory stirred cell tests.

3) The hydrodynamic conditions at the membrane surface are an important factor in the formation of the NOM gel layer. The difference in operating in a crossflow vs. dead-end filtration system produces a significant change in the hydrodynamics at the membrane surface.

For bench- and pilot-scale tests, the feedwater flows across a narrow channel (0.01 cm in height) above the membrane surface. Application of the same driving pressure and feedwater velocity across the narrow spacer material should produce fairly consistent hydrodynamic conditions across the membrane surface for bench- and pilot-scale tests.

In contrast, a stirred column of bulk feedwater solution is applied directly to the membrane surface in the laboratory stirred cell test apparatus. The stirring action moves the feedwater in a circular pattern around the circular membrane surface. The angular velocity of the feedwater increases with the radial distance from the center of the membrane. The unknown flow dynamics of the large column coupled with the radial variation in flow velocity produced hydrodynamic conditions at the membrane surface that were difficult to quantify and correlate with the crossflow hydrodynamics of bench- and pilot-scale tests.

4) All three scales of testing used microfiltration (0.30 - 0.45 μm) to pretreat the HT and CR feedwaters. The longer test periods employed in the pilot-scale tests required the addition of sulfuric acid and chloramines to prevent scaling and biofouling, respectively. The relatively small dose of sulfuric acid was not expected to affect the rate

of NOM fouling. The potential impact of chloramines on NOM fouling, however, is unknown. Chloramines represent a weak oxidant that is potentially capable of reacting with NOM, but the degree and type of potential reactions were not investigated in this research.

5) Membrane permeate in spiral-wound pilot elements travels a significant distance through tightly rolled membrane sheets before exiting to ambient pressure. This contrasts sharply with the immediate exit of permeate flow to ambient pressure that is inherent in the stirred cell and bench-scale test apparatus.

The considerable length and restricted channel height of the permeate stream at the pilot scale imposes greater drag forces than those observed at lower scales of testing using flat sheets. These friction forces are seen as additional hydraulic membrane resistance which consume a portion of the applied transmembrane pressure. They result in lower permeate flux and a corresponding decrease in the NOM mass loading as compared to stirred cell and bench-scale operations.

6) Variability in the applied pressure and NOM concentration in the feedwater affects the dynamics of NOM fouling. The amount of applied pressure was easily and carefully controlled in the stirred cell

and bench-scale tests. Pilot-scale controls, however, were not adequate to ensure consistency in applied pressure.

Temporal differences between scales of testing resulted in minor variations of NOM concentration in the feedwaters. It is expected that the consequence of variability in NOM concentration and applied pressure is increased scatter of test results.

6.6.3 Comparison of Membrane Performance

The performance and modeling parameters for all tests conducted are summarized in Table 6.19. Membrane performance is described in terms of the rate and amount of NOM gel layer formation, and is correlated with the gel resistance modeling parameters. The gel resistance model calculates the rate and amount of gel resistance in terms of the NOM mass loading (W) and the cumulative effect of all NOM-membrane interactions (K). The model was based on the assumption and intent of the experimental methodology to minimize differences in the operational parameters that also influence NOM fouling.

As discussed in the previous section, however, dynamic similarity between scales of operation was compromised to varying degrees by operational differences. The membrane performance and modeling

Table 6.19 Summary of Membrane Performance

Test	Clean Membrane Resistance R_m (m^{-1})	Uncertainty *%	Maximum Gel Resistance ** R_{max} (m^{-1})	Uncertainty *%	Gel Formation Rate*** Δt (hr)	NOM Loading W (mg C/m^2hr)	Uncertainty *%	NOM Accum. Coefficient K (m•hr/mg)	Uncertainty *%
Stirred Cell									
EH	4.5E+13	9.0	N/A		10	110 - 820	7.8 - 8.0	0.18E+11	84 (2.6)
GH	4.5E+13	9.0	N/A		14	80 - 480	8.4 - 9.0	0.23E+11	120 (4.6)
EC	4.5E+13	9.0	N/A		3	160 - 900	7.8 - 8.0	0.40E+11	73 (4.9)
GC	4.2E+13	9.0	N/A		12	80 - 470	8.9 - 10	0.40E+11	120 (6.3)
Bench Scale									
EH	4.4E+13	9.5	0.93E+13	42 (25)	50	85	11 (20)	1.1E+11	43 (32)
GH	2.3E+13	9.5	1.1E+13	33 (24)	60	120	12 (13)	0.92E+11	35 (27)
EC	4.1E+13	9.6	2.3E+13	30 (38)	3	120	11 (14)	1.9E+11	32 (40)
GC	2.7E+13	9.5	1.5E+13	30 (29)	6	69	18 (17)	2.2E+11	35 (33)
Pilot Scale									
EH	7.5E+13	9.0	1.9E+13	48 (8.6)	140	77	10 (3.5)	2.5E+11	49 (9.2)
GH	2.4E+13	9.0	1.5E+13	22 (7.7)	130	81	12 (25)	1.9E+11	25 (19)
EC	7.5E+13	9.1	3.8E+13	31 (17)	10	38	12 (27)	10E+11	34 (32)
GC	2.4E+13	9.6	2.1E+13	20 (9.0)	60	46	13 (25)	4.5E+11	24 (26)

*Uncertainty determined through propagation analysis shown without parenthesis; statistical least squares uncertainty shown within parenthesis.

** Maximum gel resistance at steady state. Stirred cell tests did not reach steady state.

*** Gel formation rate is length of time (Δt) for gel resistance to reach $1x10^{13}$ m^{-1}.

parameters are, therefore, compared with regard to the similarities and differences between the scales of operation.

The clean membrane resistance, R_m, varied between scales of testing. The membrane resistance of the pilot-scale ESNA membrane was about double the value observed at the stirred cell and bench-scale. This difference may be attributed to the greater length and/or tighter construction of the spiral wound elements which impose additional friction forces on the permeate flow. This scale-up effect was not observed for the GM membrane. Perhaps the ESNA membrane elements are more tightly wound than the GM elements. The hydraulic resistance of the GM membrane in the stirred cell tests was about double the value observed at the bench- and pilot-scale. This difference is not accounted for by operational conditions and, therefore, is likely the result of local variations in membrane permeability that are sometimes, encountered within a single membrane element.

The test data indicate a trend of decreasing NOM mass loading with increasing scale of operation. This trend is explained in terms of the operating conditions imposed at each scale of operation. The very large mass loading rates for the stirred cell tests are a consequence of the dead-end filtration mode of operation. The decreased levels of NOM loading observed at the pilot scale are due to a combination of lower applied

pressure, lower NOM concentration in the bulk feedwater, and higher membrane resistance.

A scale-up trend is apparent in the calculated values of the NOM accumulation coefficient, K. The bench-scale K values are approximately five times greater than the corresponding K values for the laboratory stirred cell tests. Similarly, pilot-scale K values are about double the corresponding K values for the bench-scale tests. The NOM accumulation coefficient is a modeling parameter that was defined in terms of properties of the feedwater, NOM, and membrane. A conclusive explanation for the scale-up trend is not discernable from operating conditions or parameter definition; however, possible explanations include:

1) The addition of chloramines to the feedwater of the pilot-scale tests may have chemically altered the NOM properties relative to stirred cell and bench-scale tests.

2) Dead-end filtration in the laboratory stirred cell tests significantly altered the concentrations of NOM and other solutes in the bulk feedwater and at the membrane surface relative to bench- and pilot-scale tests.

3) The radial stirred flow of the feedwater column in the laboratory stirred cell tests probably created very different hydrodynamic conditions at the membrane surface relative to the crossflow dynamics of bench- and pilot-scale tests. These different hydrodynamic conditions may have altered the degree of NOM-membrane interactions.

4) A biofilm may have developed on the membrane surface in proportion to the length of time tested. Test times for stirred cell, bench scale, and pilot scale were approximately 15, 300, and 500 hours, respectively. The short duration of the stirred cell tests likely precluded significant biofilm formation. Previous bench-scale research (Cho, 1998) using HT and other surface waters analyzed fouled membrane surfaces using ATR-FTIR spectroscopy and found predominantly NOM foulants but also relatively minor amounts of biological residuals (polysaccharides). Greater K values at the bench and pilot scales may be the result of a thin biofilm and/or increased NOM adsorption due to the presence of the biofilm. If so, then K values may also be dependant on the length of testing and should be considered when extrapolating data.

The maximum gel resistance values, are about 1.5 - 2 times greater for pilot-scale tests as compared to bench-scale tests. This trend correlates

well with the corresponding scale-up of K values which describe the amount of NOM mass that is incorporated into the gel layer. The plots of NOM gel resistance, R_g, increase exponentially with time and approach a maximum steady value, R_{max}, for all four source water-membrane combinations for both bench- and pilot-scale tests. For bench-scale tests, however, R_{max} was achieved more rapidly and exhibited a more constant, steady-state value than was observed in the pilot-scale tests. There are two possible explanations:

1) The bench-scale tests employed a continuous batch recycle of the permeate and concentrate streams into the feedwater reservoir (during which the finite fraction of NOM susceptible to fouling may have been gradually depleted. If this occurred, it would have resulted in a relatively more rapid approach to and constant level of R_{max}, as opposed to pilot-scale tests conducted with a single pass of feedwater through the membrane.

2) The rate of gel layer formation generally decreases with increasing scale of operation. This trend may be attributed to the decreasing trend of NOM mass loading that was observed between the scales of operation. The different operating circumstances discussed earlier in the scale-up comparison of K values may also be a factor in the scale differences of the rate of gel layer formation (e.g., lower flux at the pilot-scale due to greater friction losses in the permeate stream). The

exponential increase toward a steady value of gel resistance for single-pass systems was also observed by other researchers (Wiesner and Aptel, 1996).

A basic premise of the gel resistance model and the membrane testing protocol was to focus on NOM fouling and, therefore, eliminate other potential sources of fouling. Microfiltration of the feedwater (0.30 - 0.45 pm) provided a removal mechanism for particles and biological contaminants at all three scales of testing. The risk of biofouling was minimal for the stirred cell tests due to their short-term duration (about 16 hours).

There was a potential for biofouling of bench-scale tests due to the longer-term (about 300 hours) and continuous recycle of the concentrate and permeate streams into the bulk feedwater. A previous study using the same equipment and test conditions, however, determined that biofouling did not occur by examining the fouled membranes using scanning electronic microscopy and attenuated total reflection-Fourier transform infrared spectroscopy (Cho, 1998). At the pilot-scale level, chloramine disinfectant was added to the feedwater (0.10 mg/L) as an additional measure to preclude biofouling. All of the increase in resistance to permeate flux that occurred during membrane testing with the source waters was attributed to NOM fouling and carried through the modeling analysis. It is believed that biofouling was not a significant factor in any of the tests conducted; however,

if it did occur then it would have been included within the calculated values of gel resistance and interpreted as such.

7.0 SUMMARY AND CONCLUSIONS

A model of NOM gel resistance was developed to evaluate NOM fouling in terms of NOM-membrane interactions at different scales of membrane operation. The rate and extent of NOM gel layer formation depends on a complex interaction between the NOM, membrane, and feedwater constituents as well as numerous extrinsic factors imposed by operating conditions. Differences in operating conditions were minimized and simplifying assumptions were made regarding NOM transport to create a model that describes gel layer formation as a function of two parameters:

1) The NOM concentration near the membrane surface and,

2) The cumulative NOM-membrane interactions that promote NOM accumulation in the gel layer.

The NOM concentration proximate to the membrane surface primarily depends on the rejection characteristics of the NOM solute-membrane combination. The quantity of rejected NOM is easily calculated as the difference in NOM concentration between the bulk feedwater and permeate streams multiplied by the flux rate through the membrane. This calculated quantity of rejected NOM is referred to as the NOM mass loading, W. Although the NOM mass loading is not the precise concentration at the

membrane surface, it provides a reasonable approximation for modeling purposes. The gel resistance model was developed based on the assumption that influences from operational differences were minimized to insignificant levels. The concept of NOM mass loading, however, provides the means to account for variations in NOM concentration and permeate flux rate during each test and when comparing different tests.

It makes sense intuitively that each feedwater-membrane combination produces a unique interaction that determines the fraction of available NOM mass loading that is incorporated into the gel layer. This concept is embodied in the gel resistance model by the NOM accumulation coefficient, K. By definition, K represents the aggregate influence of NOM-membrane interactions on gel layer formation. This research did not investigate a means for measuring K based on properties of the NOM, feedwater, and membrane. Instead K is calculated indirectly from the model as the ratio of gel resistance to NOM mass loading.

The definitions and assumptions used in developing the gel resistance model indicate that both modeling parameters (Wand K) are dependant on properties of the NOM, feedwater, and membrane. The concentration and size of NOM macromolecules, and the membrane pore size, are primarily accounted for as NOM rejection using the NOM mass loading function, W. Hydrophobic and electrostatic properties of the NOM, feedwater, and

membrane are primarily accounted for by adsorption using the NOM accumulation coefficient. K.

It is hypothesized that the same properties of the NOM that promote fouling can be quantitatively correlated with K, which was defined (Eq. [5.15]) as being directly proportional to the specific resistance, α, of the NOM and inversely proportional to the rate of backtransport, A. For example, increasing hydrophobic character of NOM is expected to result in increasing K values (i.e., greater fouling). This could be interpreted as either an increase in the specific resistance of the gel layer or a decrease in the rate of backtransport. Experimental studies using different NOM sources could provide an empirical correlation between hydrophobic character (as measured by SUVA) and the NOM accumulation coefficient, K. Clearly. the gel resistance model developed herein provides theoretical insights into some aspects of the dynamics of gel layer formation as opposed to an empirical, black-box approach to modeling.

The gel resistance model has the flexibility to accommodate the different types of NOM mass loading encountered in laboratory stirred cell, bench-scale, and pilot-scale tests. For all tests conducted at each scale of testing, the form (curve fit) of the modeled gel resistance correlated well with the actual measured gel resistance values. The curve-fitting process yielded model parameters that correlated well with the measured properties of each

feedwater-membrane combination and their expected influence on NOM gel layer formation within each scale of operation.

It was hypothesized that NOM gel resistance would be greater for membrane tests using CR water as opposed to HT water due to the much greater ionic strength of the CR water. This hypothesis was corroborated by the gel resistance test data and modeling parameters for all tests conducted. A quantitative description of the influence of NOM-membrane interactions was provided by the NOM accumulation coefficient, K. The K values for CR tests were consistently about double the K values for the HT tests at each scale of operation.

A comparison of the gel resistance data and modeling parameters identified trends between the different scales of testing. A number of operational differences that might account for these trends were noted but there was insufficient information to support the selection of any particular scale-up mechanism. The gel resistance model in its present form is not a predictive model; its primary value, rather, lies in it ability to simulate gel resistance and provide insight into the NOM-membrane interactions which influence its formation.

The gel resistance model does hold promise as a potential tool for predicting NOM fouling. The potential predictive utility of the gel resistance

model would be better defined by conducting additional tests to confirm the observed trends and determine the system properties responsible for them. The results of future research could clarify the relationship between system properties and model parameters and enable water treatment utilities to utilize the model to predict performance at larger scales of operation. Specific recommendations for future research to improve the gel resistance model include:

- Study the effect (if any) of varying the input loading function, W, on the NOM accumulation coefficient, K. This would determine whether K and Ware, in fact, independent of each other, and the range of W over which the assumption of independence is valid.

- Study a range of values for each of the properties of the feedwater, NOM, and membrane which affect NOM fouling to determine their correlation with the K value. For example, vary the ionic strength (through the addition of dissolved salts) across a wide range of values for each source water-membrane combination. This should yield an empirical relationship between the ionic strength and the corresponding K value. The current study evaluated only two different ionic strengths.

- Conduct replicates of each test to determine variation in test results due to experimental error. This would establish the confidence intervals over which the test data can be applied. The current study did not conduct replicate tests.

- Study the mechanical differences between each scale of testing to determine their influence on test results. The current study identified these differences but did not investigate their influence on scale-up of membrane performance.

8.0 REFERENCES

Allgeier, Steven, C., 1999, "ICR Membrane Studies: Status Update and Data Analysis," *1999 Membrane Technology Conference Proceedings,* American Water Works Association, Long Beach, California.

AWWA Membrane Technology Research Committee, 1998, "Committee Report: Membrane Processes, *Journal of the American* Wafer *Works Association,* Vol. 89, No. 6; 91 - 105.

Bowen, W. Richard, and Frank Jenner, 1995, "Theoretical Descriptions of Membrane Filtration of Colloids and Fine Particles: An Assessment and Review," *Advances in Colloid and Interface Science,* Vol. 56; 141 - 200.

Box, George E.P., William G. Hunter, and J. Stuart Hunter, *1978, Statistics for Experimenters,* John Wiley & Sons, Inc., New York, New York; 556 - 583.

Braghetta, Anne, Francis A. DiGiano, and William P. Ball, 1998, "NOM Accumulation at NF Membrane Surface: Impact of Chemistry and Shear," *Journal of Environmental Engineering,* Vol. 141, No. 11; 1087 - 1097.

Elraghetta, Anne, Francis A. DiGiano, and William P. Ball, 1997, "Nanofrltration of Natural Organic Matter: pH and Ionic Strength Effects," *Journal of Environmental Engineering,* Vol. 123, No. 7; 628 - 641.

Chapman-Wilbert, Michelle, Frank Leitz, Ellen Abart, Bill Boegli, and Kim Linton, *1998, The Desalting and Water Treatment Membrane* **Manual:** *A Guide to Membranes for Municipal Water Treatment,* 2nd Edition, Report No. R-98-5, U.S. Bureau of Reclamation, Denver, Colorado; 9.6-9.11.

Chapra, Steven, 1997, *Surface* **Wafer-Qualify** *Modeling,* McGraw-Hill, Inc.; 67 - 85.

Cho, Jaeweon, *1998, Natural Organic Matter Rejection by, and Flux Decline of, Nanofiltration and Ultrafiltration Membranes,* doctoral dissertation, Department of Civil, Environmental, and Architectural Engineering, University of Colorado at Boulder.

DiGiano, Francis A., Anne Braghetta, James Nilson, and Bruce Utne, 1993, "Nanofiltration Fouling by Natural Organic Matter," *1993 Membrane Technology Conference Proceedings,* American Water Works Association, Baltimore, Maryland; 320 - 328.

Faust, Samuel D., and Osman M. Aly, 1998, *Chemistry of Wafer Treafmenf,* 2nd Edition, Ann Arbor Press, Chelsea, Michigan; 135 - 140 and 218 - *223.*

Fu P., H. Ruiz, K. Thompson, and C. Spangenberg, 1994, "Selecting Membranes for Removing NOM and DBP Precursors," Journal *of the American Wafer Works Association,* Vol. 86, No. 1; 55-72.

Gusses, Alison M., Steven C. Allgeier, Thomas F. Speth, and R. Scott Summers, 1996, "Verification and Use of the Rapid Bench-Scale Membrane Test," *Proceedings of the American Water Works Association Annual Conference,* Ontario, Canada.

Gusses, Alison M., Thomas F. Speth, Steven C. Allgeier, and R. Scott Summers, 1997, "Evaluation of Surface Water Pretreatment Processes Using the Rapid Bench-Scale Membrane Test," *1997 Membrane Technology Conference Proceedings,* American Water Works Association, New Orleans, Louisiana; 765 - 782.

Gusses, Alison M., Steven C. Allgeier, Thomas F. Speth, and R. Scott Summers, 1999, "Impact of Membrane Sample Variability on the Performance of the Rapid Bench-Scale Membrane Test," 7999 *Membrane Technology Conference Proceedings,* American Water Works Association, Long Beach, California.

Ho, W.S. Winston, and Kamalesh K. Sirkar, Editors, *1992, Membrane Handbook,* Van Nostrand Reinhold, New York, New York.

Himmelblau, David M., *1970, Process Analysis by Statistical Methods,* John Wiley & Sons, Inc., New York, New York; 14 - 40.

Ibrahim, Eva, Jim Lozier, and Russell Ford, 1999, "ICR Pilot Test Using an Organic Selective Nanofiltration Membrane to Treat Microfiltered Surface Water," *7999 Membrane Technology Conference Proceedings,* American Water Works Association, Long Beach, California.

Jucker, C., and Mark M. Clark, 1994, "Adsorption of Aquatic Humic Substances on Hydrophobic Ultrafiltration Membranes," *Journal of* Membrane *Science,* Vol. 97, 37 - 52.

Kennedy, John B, and Adam M. Neville, 1976, *Basic Statistical Methods for Engineers* and *Scientists,* 2nd Edition, Harper & Row, Publishers, Inc., New York, New York; 239 - 244.

Krasner, Stuart W., Zaid K. Chowdhury, Marc A. Edwards, Kimberly A. Bell, 1999, "Use of SUVA in Developing Revised TOC Removal Requirements," *7999 Membrane Technology Conference Proceedings,* American Water Works Association, Long Beach, California.

Lindeburg, Michael R., *1992, Civil Engineering Reference Manual.* 6th Edition, Professional Publications, Inc., Belmont, California; 3-38.

Mulford, Luke A., and James S. Taylor, 1997, "Verification of Single Element and Pilot Testing for ICR Compliance," *7997 Membrane Technology Conference Proceedings,* American Water Works Association, New Orleans, Louisiana; 519 - 536.

Nilson, J., and Francis A. DiGiano, 1996, "Influence of NOM Composition on Nanofiltration," *Journal of the American Wafer Works Association,* Vol. *88, No. 1, 53-66.*

O'Neil, Peter V., 1991, *Advanced Engineering Mathematics,* Wadsworth Publishing Company, Belmont, California; 65 - 70.

Porter, Mark C., 1972, "Concentration Polarization with Membrane Ultrafiltration," *Ind. Eng. Chem. Prod. Res. Develop.,* Vol 11, No. 3; *234 - 248.*

Schafer, A. I., A.G. Fane, and T.D. Waite, 1998, "Nanofiltration of Natural Organic Matter: Removal, Fouling, and the Influence of Multivalent Ions," Desalination, Vol. 118; 109 - 122.

Taylor, James S., and Ed P. Jacobs, 1996, "Reverse Osmosis and Nanofiltration," Chapter *9* of *Water Treatment Membrane Processes,* American Water Works Association Research Foundation, Lyonnaise des Eaux, and Water Research Commission of South Africa, McGraw-Hill; 9.18 - 9.20.

Tighe, James, and John Pellegrino, 1998, "Parametric Analysis of the Propagation of Uncertainty in Sorption Measurements Made with a Pressure-Decay Apparatus," *Separation Science and Technology,* Vol. 33, No. 10; 1387 - 1405.

Tu, Shih-Chieh, Varadarajan Ravindran, and Badri N. Badriyha, 1997, "'A Membrane Transport Model for Predicting Permeate Flux in Nanofiltration Processes," *7997 Membrane Technology Conference Proceedings,* American Water Works Association, New Orleans, Louisiana; 487 - 498.

U.S. Environmental Protection Agency, 1996a, "National Primary Drinking Water Regulations: Monitoring Requirements for Public Drinking Water Supplies; Final Rule," *Federal Register,* 61:94:24354 (May 14, 1996).

U.S. Environmental Protection Agency, 1996b, */CR Manual for Bench- and Pilot-Scale Treatment Studies,* EPA 814-B-96-003, Office of Water, Cincinnati, Ohio; 1-5.

Van der Meer, W.G.J., C.W. Aeijelts Averink, and J.S. van Dijk, 1997, "Mathematical Modeling of Spiral-Wound Nanofiltration Modules," *1997 Membrane Technology Conference Proceedings,* American Water Works Association, New Orleans, Louisiana; 499 - 517.

Weast, Robert C., David R. Lide, Melvin J. Astle, and William H. Beyer, Editors, *CRC Handbook of Chemistry and Physics,* CRC Press, Boca Raton, Florida; D-255.

White, Frank M., *1986, Fluid Mechanics,* 2nd Edition, McGraw-Hill Book Co.; 28.

Wiesner, Mark R., and P. Aptel, 1996, "Reverse Osmosis and Nanofiltration," Chapter *4* of *Water Treatment Membrane Processes,* American Water Works Association Research Foundation, Lyonnaise des Eaux, and Water Research Commission of South Africa, McGraw-Hill; 4.16 - 4.28.

Wiesner, Mark R., and S. Chellam, 1992, "Mass Transport Considerations for Pressure-Driven Membrane Processes," *Journal of the American Water Works Association,* Vol. 84; 88 - 95.

Zhang, W., M. Wahgren, and B. Sivik, 1989, "Membrane Characterization by the Contact Angle Technique II," *Desalination,* Vol. 72; 263 - 273.

APPENDIX

Laboratory Data for Initial Clean Water Flux

Table A.1 Laboratory Data for Initial Clean Water Flux

Test	Time (hr)	Temp. (°C)	Absolute Viscosity (Pa*s)	Permeate Flow, C! (mL/min)	Normalized Flux, J ($L/m^2/hr$)	Membrane Resistance (m^{-1})
Stirred Cell						
EH	3	25.1	9.09E-04	2.13	42.3	4.49E+13
GH	3	27.2	8.66E-04	2.12	42.1	4.51E+13
EC	3	23.3	9.48E-04	2.14	42.5	4.46E+13
GC	3	24.8	9.15E-04	2.27	45.1	4.21E+13
Bench						
EH	0.0	27.2	8.66E-04	12.1	43.9	4.33E+13
	10.5	24.9	9.13E-04	11.2	43.5	4.43E+13
	10.9	25.0	9.11E-04	11.3	43.8	4.41E+13
	11.1	25.1	9.09E-04	11.3	43.7	4.42E+13
	11.3	25.3	9.05E-04	11.4	43.8	4.40E+13
	11.5	25.4	9.02E-04	11.4	43.7	4.41E+13
GH	0.0	22.1	9.76E-04	19.6	82.8	2.19E+13
	0.5	22.4	9.69E-04	19.2	80.4	2.24E+13
	1.5	22.9	9.57E-04	18.7	77.1	2.31E+13
	12.0	25.4	9.02E-04	19.1	73.7	2.38E+13
	23.0	22.5	9.66E-04	18.7	78.0	2.29E+13
	23.3	22.4	9.69E-04	18.6	77.9	2.30E+13
EC	0.0	22.2	9.73E-04	15.9	66.9	3.85E+13
	0.2	22.5	9.66E-04	15.6	65.1	3.92E+13
	0.4	22.8	9.59E-04	15.5	64.1	3.96E+13
	2.3	24.5	9.22E-04	15.4	60.6	4.11E+13
GC	0	26.7	8.76E-04	20.8	76.7	2.48E+13
	3.2	28.8	8.36E-04	19.8	68.6	2.66E+13
	7	30.1	8.12E-04	20	66.7	2.69E+13
	15.5	24.6	9.19E-04	18.1	71.0	2.64E+13
	16.0	24.4	9.24E-04	18	71.0	2.65E+13
Pilot						
EH	0.0	22.7	9.62E-04	1290	31.9	7.28E+13
	1.0	22.7	9.62E-04	1300	32.1	7.23E+13
	2.0	22.8	9.59E-04	1260	31.0	7.44E+13
	4.0	22.7	9.62E-04	1260	31.1	7.42E+13
	6.0	22.7	9.62E-04	1250	30.9	7.47E+13
	10.0	22.7	9.62E-04	1250	30.9	7.47E+13
GH	0.0	22.6	9.64E-04	2190	54.3	2.28E+13
	1.0	22.7	9.62E-04	2150	53.1	2.33E+13
	2.0	22.7	9.62E-04	2110	52.1	2.38E+13
	4.0	22.6	9.64E-04	2100	52.0	2.39E+13
	6.0	22.7	9.62E-04	2120	52.4	2.37E+13
	10.0	22.7	9.62E-04	2110	52.1	2.38E+13
EC	24	32.0	7.79E-04	930	17.5	7.52E+13
GC	24	32.0	7.79E-04	2110	39.6	2.40E+13